Novel tRNA-like transcripts from the NEAT1-MALAT1 genomic region critically influence human innate immunity and macrophage functions

Martina Gast
Charite Universitätsmedizin Berlin
Vanasa Nageswaran
Charite Universitätsmedizin Berlin
Andreas Kuss
Department of Functional Genomics, Interfaculty Institute of Genetics and Functional Genomics
Ana Tzvetkova
Department of Functional Genomics, Interfaculty Institute of Genetics and Functional Genomics
Xiaomin Wang
Charite Universitätsmedizin Berlin
Liliana Mochmann
Pathologisches Institut Ludwig-Maximilians Universität
Pegah Ramezani-Rad
Charite Universitätsmedizin Berlin
Stefan Weiss
University Medicine Greifswald & University of Greifswald https://orcid.org/0000-0002-3553-4315
Stefan Simm
Institute of Bioinformatics, University Medicine Greifswald
Tanja Zeller
UKE Hamburg https://orcid.org/0000-0003-3379-2641
Henry Voelzke
Institute for Community Medicine, University Medicine Greifswald
Wolfgang Hoffmann
Institute for Community Medicine, University Medicine Greifswald
Uwe Völker
Department of Functional Genomics, Interfaculty Institute of Genetics and Functional Genomics, University Medicine Greifswald
Stefan Felix
Department of Cardiology, University Medicine Greifswald
Marcus Dörr
Department of Cardiology, University Medicine Greifswald

Antje Beling
Charite Universitätsmedizin Berlin
Carsten Skurk
Charite Universitätsmedizin Berlin
David-Manuel Leistner
Charite Universitätsmedizin Berlin
Bernhard Rauch
Department Human Medicine, Section Pharmacology and Toxicology, Carl von Ossietzky Universität
Tetsuro Hirose
Graduate School of Frontier Biosciences, Osaka University
Bettina Heidecker
Charité Universitätsmedizin Berlin
Karin Klingel
University Hospital Tübingen
Shinichi Nakagawa
RNA Biology Laboratory Faculty of Pharmaceutical Sciences, Hokkaido University
Wolfram Poller
Icahn School of Medicine at Mount Sinai https://orcid.org/0000-0002-4632-5551
Filip Swirski
Icahn School of Medicine at Mount Sinai https://orcid.org/0000-0002-3163-9152
Arash Haghikia
Charite - Universitätsmedizin Berlin
Wolfgang Poller (wolfgang.poller@charite.de)
Charite Universitätsmedizin Berlin https://orcid.org/0000-0002-2805-6634

Article

Keywords: Immunology, innate immunity, immunogenetics, noncoding genome, tRNA biology, evolutionary genetics

Posted Date: April 21st, 2022

DOI: https://doi.org/10.21203/rs.3.rs-1540419/v2

Novel tRNA-like transcripts from the *NEAT1-MALAT1* genomic region critically influence human innate immunity and macrophage functions

Martina Gast [1,2 #], Vanasa Nageswaran [1,3 #], Andreas W. Kuss [4 #], Ana Tzvetkova [4,5], Xiaomin Wang [1], Liliana H. Mochmann [1], Pegah Ramezani Rad [1], Stefan Weiss [4,6], Stefan Simm [5], Tanja Zeller [7,8], Henry Voelzke [6,9], Wolfgang Hoffmann [6,9], Uwe Völker [4,6], Stefan B. Felix [6,10], Marcus Dörr [6,10], Antje Beling [2,11,12], Carsten Skurk [1,2], David-Manuel Leistner [1,2,12], Bernhard H. Rauch [6,13,14], Tetsuro Hirose [15], Bettina Heidecker [1], Karin Klingel [16], Shinichi Nakagawa [17,18], Wolfram C. Poller [19,20], Filip K. Swirski [19,20], Arash Haghikia [1,2,12 #], Wolfgang Poller [1,2,21 # §]

[1] Department of Cardiology, Campus *Benjamin Franklin*; [11] Institute for Biochemistry; and [21] Berlin-Brandenburg Center for Regenerative Therapies (BCRT), all at Charité - Universitätsmedizin Berlin, Charité-Universitätsmedizin Berlin, corporate member of Freie Universität Berlin, Humboldt-Universität zu Berlin, and Berlin Institute of Health, Berlin, Germany.

[3] Institute for Chemistry and Biochemistry, Freie Universität Berlin, Berlin, Germany.

[4] Department of Functional Genomics, Interfaculty Institute of Genetics and Functional Genomics; and [5] Institute of Bioinformatics, both at University Medicine Greifswald, Greifswald, Germany.

[7] University Center of Cardiovascular Science, University Heart and Vascular Center, Hamburg, Germany.

[9] Institute for Community Medicine, University Medicine Greifswald, Greifswald, Germany.

[10] Department of Cardiology, University Medicine Greifswald, Greifswald, Germany.

[12] Berlin Institute of Health (BIH), Berlin, Germany.

[13] Institute for Pharmacology, University Medicine Greifswald, Greifswald, Germany.

[14] Department Human Medicine, Section Pharmacology and Toxicology, Carl von Ossietzky Universität, Oldenburg, Germany.

[15] Graduate School of Frontier Biosciences, Osaka University, 1-3 Yamadaoka, Suita 565-0871, Japan.

[16] Institute for Pathology and Neuropathology, Department of Pathology, University Hospital Tübingen, Germany.

[17] RNA Biology Laboratory, RIKEN Advanced Research Institute, Wako, Saitama, Japan.

[18] Faculty of Pharmaceutical Sciences, Hokkaido University, Sapporo, Japan.

[19] Center for Systems Biology, Massachusetts General Hospital and Harvard Medical School, MA, USA.

[20] Cardiovascular Research Institute, Icahn School of Medicine at Mount Sinai, New York, NY, USA

German Center for Cardiovascular Research (DZHK) [2] Site Berlin, [6] Site Greifswald, [8] Site Hamburg/Lübeck/Kiel, Germany.

[#] equal contributions [§] correspondence

Running Title: A novel class of tRNA-like small noncoding RNAs

Keywords: Immunology; innate immunity; immunogenetics; noncoding genome; tRNA biology; evolutionary genetics

Correspondence:
Wolfgang Ch. Poller *M.D.*
Phone +49-30-450-613765
Fax +49-30-450-7-513984
wolfgang.poller@charite.de

Abstract

The evolutionary conserved *NEAT1-MALAT1* gene cluster generates large noncoding transcripts remaining nuclear, while tRNA-like transcripts (mascRNA, menRNA) enzymatically generated from these precursors translocate to the cytosol. *NEAT1*$^{-/-}$ and *MALAT1*$^{-/-}$ mice display massive atherosclerosis and vascular inflammation.

Here, we identify the tRNA-like molecules as critical components of innate immunity. They appear as prototypes of a new class of noncoding RNAs distinct from others (miRNAs, siRNAs) by biosynthetic pathway and intracellular kinetics. CRISPR-generated human ΔmascRNA and ΔmenRNA monocytes/macrophages display defective innate immune sensing, loss of cytokine control, imbalance of growth/angiogenic factor expression impacting upon angiogenesis, and altered cell-cell interaction systems. Antiviral response, foam cell formation/oxLDL uptake, and M1/M2 polarization are defective in ΔmascRNA/ΔmenRNA macrophages, defining the tRNA-like molecules' first described biological functions.

menRNA and mascRNA represent novel components of innate immunity arising from the noncoding genome. Their *NEAT1-MALAT1* region of origin appears as archetype of a functionally highly integrated RNA processing system.

The evolutionary conserved *NEAT1-MALAT1* cluster encounters high interest in both cardiovascular medicine and oncology. In the cardiovascular field, we observed suppression of lncRNA *NEAT1* in circulating immune cells of post-myocardial infarction (MI) patients [1]. Mice lacking lncRNAs *NEAT1* [1] or *MALAT1* [2-4] displayed immune disturbances affecting monocyte-macrophage and T cell differentiation and rendering the immune system highly vulnerable to stress stimuli, thereby promoting the development of atherosclerosis. Uncontrolled inflammation is also a key driver of multiple other diseases [1,2,4-6].

Here, we report the first biological functions of two novel tRNA-type transcripts from the *NEAT1-MALAT1* cluster (Fig. 1) and describe deep impact upon innate immunity and macrophage functions. While we previously investigated mice deficient in the entire *NEAT1* or *MALAT1* locus, we now aimed to selectively disrupt only tRNA-like transcripts 'menRNA' arising from *NEAT1* [7,8], or 'mascRNA' arising from *MALAT1.* To date, no biological function of neither one of the tRNA-like transcripts has been reported. Both lncRNAs give rise to transcripts of vastly different size (*NEAT1*: 23kb MENβ, 3.7kb MENε, 59nt 'menRNA'; *MALAT1*: 8.3 kb primary, 58nt 'mascRNA'), and traditional knockout methods are unable to selectively inactivate one of the small transcripts only. Through CRISPR-Cas9 editing [9], we therefore developed human monocyte-macrophage cell lines with short deletions in the respective tRNA-encoding sequences to disrupt normal menRNA or mascRNA formation, respectively. These editing procedures occur outside of the primary transcript sequences required for regular formation of the triple-helix structures at their 3'-ends which support stabilization of the respective lncRNAs (Fig. 1AB). The CRISPR-Cas9-based editing of menRNA or mascRNA selectively prevented only the normal transcript folding and formation of mature menRNA or mascRNA, respectively. Unlike monocytes and macrophages in *NEAT1*$^{-/-}$ mice [1], CRISPR-Cas9-generated ΔmenRNA cells retained MEN-β and MEN-ε expression. Similarly, ΔmascRNA monocytes preserved expression of the long *MALAT1* precursor while mascRNA, normally highly enriched in this cell type, became ablated.

Beyond prior work documenting immune function of the *NEAT1-MALAT1* cluster, the current study identifies menRNA and mascRNA as novel elements of innate immunity impacting upon cytokine regulation, immune cell-endothelium interactions, angiogenesis, and monocyte-macrophage differentiation and functions. These molecules are prototypes of a new class of RNAs distinct from other small transcripts (miRNAs, siRNAs) by biosynthetic pathway and intracellular kinetics. From an evolutionary perspective, the *NEAT1-MALAT1* genomic region appears as archetype of a functionally highly integrated RNA processing system.

Results

Targeted deletion of tRNA-like transcripts from the NEAT1-MALAT1 cluster

While previously investigated mice were deficient in the entire *NEAT1* or *MALAT1* locus [1,2,4], we here aimed to selectively disrupt only the novel 59-nt tRNA-like transcript 'menRNA' with so far unknown biological functions (Fig. 1A). Through CRISPR-Cas9 editing, we developed human THP-1 monocyte-macrophage cell lines with deletions of different extent all of which prevent, however, normal transcript folding and formation of menRNA or mascRNA, respectively. Unlike monocytes/macrophages in *NEAT1*$^{-/-}$ mice [1], the CRISPR/Cas9-generated ΔmenRNA cells retained apparently normal MEN-β and MEN-ε expression. Similarly, ΔmascRNA monocytes/macrophages preserved expression of the *MALAT1* precursor (Fig. 1B) whereas mascRNA, normally highly enriched in this cell type, became

ablated (Suppl. Fig. S1-S3). As a consequence of its rapid turnover, the cellular steady-state level of menRNA is very low. For this reason, the silencing efficacy of ASOs or siRNAs with regard to menRNA abundance in the cells could not be ascertained neither by RT-PCR nor Northern blot analyses (Suppl. Fig. S1C and D). Very low menRNA abundance in immune cells is in sharp contrast to the enrichment of mascRNA in monocytes first described by our group [3]. We found high efficacy of antisense oligonucleotides (ASOs) targeting the mascRNA sequence, regarding reduction of the mascRNA level in monocytes. Importantly, however, neither ASOs nor siRNAs are capable to selectively react with and thereby ablate only the 'mature' menRNA or mascRNA, respectively. Instead, they will also react with the 23kb *NEAT1* and 8.3kb *MALAT1* long precursor transcripts and mediate their premature decay, making unequivocal distinction between biological effects of menRNA/mascRNA ablation from those of *NEAT1*/*MALAT1* reduction [1,2,4] impossible. In the peculiar case of the high-turnover menRNA, the CRISPR-Cas9 deletion clone as employed here is obviously a highly specific system for selective menRNA ablation and subsequent functional assignment of cellular/biological functions to menRNA. Finally, any attempt to generate germ-line menRNA or mascRNA deficient animal models would be technically demanding and likely also display developmental/ embryonic anomalies of disturbances in somatic cells other than immune cells/monocytes. One would instead need mice with a monocyte-specific, adult-age inducible, selective knockout of the menRNA or mascRNA sequence only to resolve these issues. Beyond these technical challenges, there exists no murine homologue to human IL-8 which was, however, the most strongly deregulated cytokine in circulating immune cells of post-MI patients [1]. These ambiguities are avoided by CRISPR-mediated deletion in one specific cell type/line of human origin. We examined whether absence of menRNA in ΔmenRNA monocytes affects, by some cytosolic-nuclear feedback mechanism, the cellular expression level of *NEAT1*. Under the experimental conditions employed here, however, there was no change as detectable by RNA-sequencing (RNA-seq) and qRT-PCR.

Defective innate immune sensing by ΔmenRNA and ΔmascRNA cells

RNA-seq identified profound alterations in the baseline transcriptomes of ΔmenRNA and ΔmascRNA monocytes (Fig. 2AB, Suppl. Tables S1/S2). A prominent finding was gross dysbalance between multiple innate immune sensors in ΔmenRNA monocytes (Fig. 3AB, Table S1A), including cytosolic NOD-like receptors NOD2 [10] and CIITA [11], NLR-class receptors NLRC3, NLRC4 and MEFV [12-14], and membrane-bound Toll-like receptors (TLR1, TLR2, TLR7, TLR10). In the context of baseline induction of NOD2 and TLR2, it is notable that twist family bHLH transcription factor 2 (TWIST2) [15] was ~10-fold down in ΔmenRNA cells (Fig. 3GH), and loss of NLRC3 and TWIST2 expression in ΔmenRNA monocytes could not be rescued by LPS (Fig. 3E)(compare Fig. 6A. ΔmascRNA monocytes displayed induction of interferon (IFN)-induced transmembrane (IFITM) proteins [16](Fig. 3C, Table S2A).

Transcription, translation, and epigenome level anomalies in defective monocytes

Transcription and nuclear factors and epigenome modifiers (Fig. 3G-I, Tables S1B/S2B), as well as translation factors, ribosomal proteins and nucleic acid modifiers (Fig. 3K-M, Tables S1C/S2C) were deregulated in defective cells. At the transcriptional level, in addition to TWIST2, transcription factor (TF) GATA2 was ~4-fold induced and GATA6 ~20-fold suppressed, and NFATC2 switched off in ΔmenRNA cells (Fig. 3G). Further TFs and epigenome modifiers turned into disequilibrium upon LPS challenge (Fig. 3H), among them histone deacetylases, lysine demethylases, and METTL methyltransferases [17]. At the level of translation, three initiation and elongation-related factors (EIF3CL, EEF1A2, CTIF)

were induced while initiation factor EIF1AY [18] and ribosomal protein RPS4Y1 were switched off in ΔmenRNA cells (Fig. 3KL). Nucleic acid-modifying enzymes deregulated include DEAD-box helicase DDX3Y (shut off), and NOP2/Sun methyltransferase NSUN7 [19-21] which is switched on in ΔmenRNA cells (Fig. 3K, Table S1C). At the level of tRNAs, genomically or mitochondrially encoded tRNAs [20,21] and tRNA methyltransferases turned into imbalance. In ΔmascRNA cells (Fig. 3M), cytosolic nucleotidase NT5C1A [22] dephosphorylating 5' and 2'(3')-phosphates of deoxyribonucleotides with broad substrate specificity, is suppressed. Furthermore, RNA-seq identified deregulation of long noncoding RNAs (lncRNAs) and antisense (AS) RNAs in ΔmenRNA and ΔmascRNA monocytes (Tables S1D/2D). Thus, ΔmenRNA cells showed ~7-fold downregulation of a recently discovered novel transcript designated 'MARCKS cis-regulating lncRNA promoter of cytokines and inflammation' or 'regulator of cytokines and inflammation' (ROCKI) (Fig. 4DE, Table S1D/S2D). This transcript of particular interest was identified by Zhang *et al.* [23] by genome-wide scan of macrophages for pairs of cis-acting lncRNAs and protein-coding genes involved in innate immunity.

Excessive inflammatory cytokine production by ΔmenRNA and ΔmascRNA cells

We found massively elevated basal expression and secretion of IL-8, TNF, and IL1B in ΔmenRNA monocytes (Fig. 4AB). ΔmascRNA monocytes displayed exaggerated LPS induction of IL1A, IL1B, IL10, and ISG15 (Fig. 4C). Conversely, ΔmenRNA but not ΔmascRNA macrophages displayed blunted NOS2 expression and impaired ROS production upon LPS or H2O2 challenge (Fig. 7C). There were anomalies of further interleukin (IL)/receptor and TNF cytokine/receptor systems (Fig. 4D-F, Tables S1E/S2E). Receptor IL4R was ~7-fold and M2 macrophage polarization regulator IL4I1 [24,25] ~11-fold down in ΔmenRNA monocytes (Fig. 4DE). Even more pronounced was disequilibrium within the IL18 system. Receptor IL18R1 and IL18 receptor accessory protein (IL18RAP) were switched off. IL2 receptor IL2R-β (IL2RB) was ~52-fold and IL2R-γ (IL2Rc) ~13-fold suppressed. IL1 receptor antagonist (IL1RN) was ~12-fold and IL1 receptor associated kinase 2 (IRAK2) ~8-fold down in ΔmenRNA cells. Among ligands, IL16 remained ~18-fold suppressed even after LPS stimulation.

'Regulator of cytokines and inflammation' (ROCKI) was ~7-fold and SLFN5, a transcriptional co-repressor of interferon (IFN) responses and antiviral restriction factor [26-29], ~10-fold suppressed in ΔmenRNA monocytes (Fig. 4DE) while another member (SLFN12L) of the SLFN family of IFN-induced genes was ~26-fold up. Several ADAM metallopeptidases (Tables S1E/S2E) as well as cluster of differentiation (CD) and other leukocyte marker proteins [30-39] (Tables S1F/S2F) were likewise deregulated and some of them switched off in ΔmenRNA (Fig. 6HI) or ΔmascRNA cells (Fig. 6K).

Disturbed growth pattern and endothelium interactions of ΔmenRNA monocytes

At the cellular level, ΔmenRNA monocytes displayed an anomalous growth pattern with spontaneous cell cluster formation in liquid culture (Fig. 5A), and defective endothelial adhesion under multiple flow conditions (Fig. 5B). The LPS-dependent induction of cell adhesion molecules (ICAM1, VCAM1) was defective in ΔmenRNA monocytes (Fig. 5C), contrasting with exacerbated induction in ΔmascRNA monocytes. ΔmenRNA monocyte-conditioned medium altered expression of multiple gene in HAEC monolayers (Fig. 5D), whereas ΔmascRNA monocyte medium had no such effect. This observation of transcriptome changes in endothelial cells under influence of the ΔmenRNA monocyte secretome prompted further studies regarding indirect influence of the anomalous monocyte clones upon endothelial

cell behaviour, mediated *via* their secretomes, or *via* interaction between the monocytes and endothelial cells in co-cultures of both cell types in matrigel (Fig. 5HI). RNA-seq identified profound deregulation of further cell adhesion molecules in ΔmenRNA monocytes (Fig. 5EF, Table S1G), including adhesion G protein-coupled receptors [40], intercellular and neural cell adhesion molecules, integrins, vascular cell adhesion molecule, melanoma cell adhesion molecule MCAM (CD146), and endothelial cell-specific adhesion molecule (ESAM). ΔmascRNA cells also displayed anomalous cell adhesion molecule expression (Fig. 5G, Table S2G), however distinct from ΔmenRNA monocytes. Neuronal growth regulator NEGR1 is ~28-fold suppressed in ΔmenRNA but unaltered in ΔmascRNA monocytes, whereas cytoskeleton regulating NCKAP1 was ~14-fold increased in ΔmascRNA while unaltered in ΔmenRNA cells. lncRNA SENCR, involved in maintenance of endothelial cell homeostasis, is ~12-fold down in ΔmenRNA monocytes (Table S2D), suggesting menRNA loss may lead to SENCR downregulation and cellular dysfunction in endothelial cells, too.

Impact of ΔmenRNA and ΔmascRNA monocytes upon angiogenesis

A quantitative effect of ΔmenRNA and ΔmascRNA monocyte-conditioned media upon HAEC-based tube formation was observed in matrigel assays. Supernatant from each of the defective cell clones significantly reduced the tube number (Fig. 5H). Beyond this quantitative effect of secreted factors from the cells, direct co-culture of ΔmenRNA as well as of ΔmascRNA monocytes with the HAECs in the matrigel assay lead to profound alterations of HAEC cell morphology (Fig. 5I). In co-cultures with either of the defective monocyte clones, there was a massive increase in the size of HAECs at branch side nodes where ≥3 endothelial cells came into contact. When the defective monocytes clones were stained red before addition to the HAEC-matrigel mixture, there was significant accumulation of red cells at branch side nodes where HAEC hypertrophy occurred (Fig. 5I). Consistent with these observations, multiple growth and angiogenesis-associated factors and chemokines [41,42] were in disequilibrium in ΔmenRNA (Fig. 5KL, Table S1H) and ΔmascRNA monocytes (Fig. 5M, Table S12H).

Response of ΔmenRNA and ΔmascRNA macrophages to human-pathogenic viruses

PMA-based *in vitro* differentiation of ΔmenRNA and ΔmascRNA monocytes into adherent macrophages rendered the cells susceptible to transduction by recombinant adenovirus expressing GFP (Suppl. Fig. S8A). Similarly, ΔmenRNA and ΔmascRNA macrophages became transducible with human coxsackievirus B3 (CVB3) and displayed an immune response to the internalized CVB3 ssRNA genome, in the absence of active CVB3 virus replication (Suppl. Fig. S8B). In ΔmenRNA macrophages, without LPS stimulation or adenovirus transduction, IL8 expression was >100-fold induced compared to controls (Fig. 6A). Adenovirus resulted in moderate IL8 decrease, while control cells retained extremely low IL8 expression upon transduction. Several other genes had significantly higher baseline expression in ΔmenRNA macrophages, either *without* response to virus (TNF, SLFN12L, NOD2, TLR2, Il1B), or with significant *further* induction upon exposure (RIG-like receptors RLR1 and RLR2, ISG 15, TGFB2). Most conspicuous was a complete shutdown of genes suppressed in ΔmenRNA monocytes (Fig. 3A-E, Fig. 4EF) already before their transformation into macrophages: NOD-like innate immune genes NLRC3 and MEFV, IL2 receptor subunits β and γ, transcription factor TWIST2, and NFATC2. None of these genes fully silenced in macrophages could be 'rescued' by adenovirus exposure (Fig. 6A), similar to findings in LPS-stimulated monocytes (Fig. 3A-E, Fig. 4EF). Fig. 6B shows the response of ΔmenRNA

macrophages to CVB3. Regarding IL8, their response to CVB3 with further IL8 induction beyond their already very high baseline level, was opposite to their anti-adenovirus reaction. ISG15 and Il1B responded similarly to CVB3 and RR5, while IRF7 and IRF9 expression were downregulated by CVB3 only. Inducible NO synthase (NOS2) expression as well as ROS production upon LPS or H2O2 challenge was significantly reduced in ΔmenRNA macrophages (Fig. 6C). Fig. 6D summarizes key defects of the antiviral response.

menRNA deletion critically disturbs scavenger receptor expression and oxLDL uptake

ΔmenRNA macrophages display loss of oxLDL uptake (Fig. 6E), consistent with their loss of scavenger receptors (Fig. 6F) [43]. ΔmenRNA cells showed further anomalies regarding receptors involved in phagocytosis: Fcγ receptors (FcγRs) [44,45] and complement receptors (CRs) (Fig. 6HI).

Defective monocyte-macrophage transition and polarization of ΔmenRNA and ΔmascRNA cells

ΔmenRNA monocytes are unable to normally differentiate into M0 macrophages upon PMA exposure (Fig. 7A). This is consistent with disturbances of CD molecule expression in these cells, including CD11b (ITGAM), CD11c (ITGAX), and CD93 [46-48]. Beyond monocyte-macrophage transition, there was defective M1/M2 polarization of ΔmenRNA and ΔmascRNA cells. Rather simple expression profiles allowed distinction between ΔmascRNA and ΔmenRNA macrophages and controls (Fig. 7BC). A "M2-like" pattern CD163^{hi} CD200R^{hi} CD206^{hi} TGFB3^{hi} TLR10^{hi} was observed in ΔmascRNA cells [49]. A profile involving IL1B, CD93, TGFB2, TLR7, CSF1 and its receptor CSF1R [50,51] unequivocally characterizes ΔmenRNA monocytes-macrophages and is preserved through polarization. Upon prolonged culture, the morphological aspect of M2-polarized ΔmenRNA cell cultures was clearly distinct from control and ΔmascRNA cells (Fig. 7E).

Genetic heterogeneity of the NEAT1-MALAT1 region in humans

Since multiple data suggests inflammation control functions of the *NEAT1-MALAT1* cluster, we investigated the extent of variability of this region in humans by screening for sequence variants in cohorts from the population-wide SHIP study. The SHIP database encompasses clinical, biochemical, and molecular genetic data from 7.500 individuals from Central Europe (Suppl. Fig. S5 and S6AB). Full sequence data for the specific target regions of the current study, *i.e.* mascRNA and menRNA, are currently unavailable for any patient cohorts, although several SNP are known to occur mascRNA and menRNA (Suppl. Fig. S4). One *MALAT1* SNP with low minor allele frequency (MAF=0.01) located in the *MALAT1* promotor was associated (p=0.0062) with systemic low level inflammation (CRP>3.0 mg/L) (Suppl. Fig. S7A).

Discussion

NEAT1 and *MALAT1* are involved in two fields of medicine (cardiovascular and malignant diseases) linked to some degree by common immune-related mechanisms [5]. A unified concept to explain the connections of this genomic region to apparently diverse diseases may be derived from recent observations regarding immunoregulatory functions of transcripts from this cluster, encompassing the current study assigning novel immune functions to both tRNA-like transcripts. Despite differences in their specific regulatory properties, it appears that the fundamental principle of 'employing' this peculiar type of small ncRNAs was evolutionarily advantageous.

Prior studies of the NEAT1-MALAT1 cluster: We reported suppression of lncRNA *NEAT1* in circulating immune cells of post-MI patients. In mice lacking lncRNAs *NEAT1* [1] or *MALAT1* [2-4] we observed immune disturbances rendering the immune system unstable and highly vulnerable to immune stress. *MALAT1*$^{-/+}$ ApoE$^{-/-}$ mice suffered accelerated atherosclerosis despite normal diet compared to ApoE$^{-/-}$ mice. *NEAT1*$^{-/-}$ mice showed anomalous T cell and monocyte-macrophage differentiation, and systemic inflammation. *NEAT1* promotes inflammasome activation in macrophages, regulates M2 polarization [52], and influences Th17/CD4^{+} T cell differentiation. *NEAT1* knockdown induces a tolerogenic phenotype in dendritic cells by inhibiting NLRP3 inflammasome activation. Further *NEAT1* or *MALAT1* related anomalies were reported in non-immune cell types: cardiomyocytes, endothelial cells, and smooth muscle cells where an HDAC9-*MALAT1*-BRG1 complex mediates dysfunction [53]. Clinically, *NEAT1* correlated with increased exacerbation risk, severity, and inflammation in asthma [54], and with worse disease condition and poor recurrence-free survival in acute ischemic stroke. *NEAT1* is elevated in peripheral blood cells of Parkinson disease patients [55] and abnormally expressed in a wide variety of human cancers [56].

Functional dissection of the NEAT1-menRNA system: A subset of lncRNAs, termed architectural RNAs (arcRNAs), function in formation and maintenance of phase-separated membraneless organelles. In the crowded intracellular environment these are important forms of compartmentalization. Thus, *NEAT1* is a well-characterized arcRNA acting as an essential scaffold of paraspeckle nuclear bodies. In contrast, no cellular or biological functions of the cytosolic menRNA or mascRNA were known so far. Synopsis of prior genetic studies of *MALAT1* and *NEAT1* with the present one delineate the *NEAT1-MALAT1* region as a highly integrated RNA processing circuitry critically contributing to immune homeostasis. Its components MEN-β, MEN-ε, menRNA, *MALAT1*, *TALAM1*, and mascRNA are obviously set for balanced interaction with each other, and genetic ablation of any element leads to major dysfunction.

Critical defects of innate immune sensing*:* One key finding in ΔmenRNA cells was deregulation of membrane-bound (TLR2) and cytosolic immune sensors (Fig. 3). NOD2 and CIITA were massively induced while NLR-class receptors NLRC3 and MEFV were shut off in ΔmenRNA cells and could be rescued neither by LPS nor virus exposure. TWIST2, a critical regulator of cytokines in human monocyte-derived macrophages [15], NFATC2 which translocates to the nucleus upon T cell receptor stimulation, and IL2 receptor subunits β and γ, were likewise shut down and not rescuable. Further, there was massive downregulation of lncRNA ROCKI, apparently resulting from mere deletion of the small 'menRNA' sequence from an otherwise intact ~23 kb *NEAT1*. An important recent study [23] discovered that ROCKI is a master regulator of inflammatory responses. Beyond the transcription level, ΔmenRNA and ΔmascRNA cells displayed major changes of their epigenomes (Fig. 3).

Loss of inflammatory cytokine control*:* ΔmenRNA and ΔmascRNA cells display anomalous antiviral responses (Fig. 5). Even in absence of infectious agents or other immune challenges, however, ΔmenRNA cells display massive inductions of IL8 and TNF (Fig. 4). Regarding IL8, clinical observational studies suggest a critical role of IL8 in cardiovascular diseases [57,58] and stroke [59]. IL8 is mechanistically involved in the innate immune response by TLR4 signaling, induces neutrophil extracellular traps (NETs) *via* activation NFκB signaling [60], mediates hyper-signaling in aortic aneurysms, and is involved in endothelial adhesion [61]. With regard to IL8, our prior transcriptome analysis of circulating immune cells from post-MI patients [1] is of interest. IL8 was the most decisively upregulated gene post-MI, contrary to an

extremely low level in healthy subjects, although all patients were receiving state-of-the-art post-MI pharmacological treatment. In that study, the long primary lncRNA transcript *NEAT1* was significantly suppressed in post-MI PBMCs. The new data from ΔmenRNA cells are consistent with the assumption that reduction of the menRNA level in PBMCs (consecutive to or independent of the observed *NEAT1* reduction) directly contributes to IL8 induction. Further, the marked IL1B induction in post-MI PBMCs would parallel the high baseline IL1B expression in ΔmenRNA cells. It would have been most interesting to directly measure menRNA levels in the post-MI PBMCs. Due to the complex secondary and tertiary structure of mature menRNA this would have required, however, Northern blot analyses for which there was insufficient RNA available in that former post-MI study. For future translational studies, our approach to study menRNA and mascRNA directly suggests new avenue since their highly dynamic levels may be more closely related to clinical parameters and clinical course than those of their nuclear precursors.

Imbalance of angiogenic factors and chemokine systems: Excessive inflammatory cytokine production appears as one downstream consequence of defective immune sensing. Imbalance of angiogenic factors, chemokines, and cell-cell adhesion molecules may be considered as further sequelae of dysfunction at the sensor level. It is not unexpected that the anomalies at this level should have far-reaching impact upon the cells' biological behavior. Thus, irrespective of differences between ΔmenRNA and ΔmascRNA cells, both significantly decreased tube formation in matrigel assay and displayed profound deregulation of cell-cell adhesion molecules (Fig. 5). In the case of ΔmenRNA cells, the latter was immediately apparent by their anomalous growth in clusters, and their defective endothelial flow adhesion to HAECs. While de-repression of multiple growth/angiogenetic factors appears directly linked to anomalous endothelial cell growth and morphology in the monocyte-endothelial cell co-cultures, this imbalance of growth/angiogenetic factors apparently does not support effective tube formation, but instead hinders it.

Defective foam cell formation and macrophage polarization*:* This occurs in the context of large-scale disturbance of the cells' immune sensors from NOD-like and Toll-like (Fig. 3) to phagocytosis-related receptors (Fig. 6). Overall, the cells are unable to adequately respond to immune challenges including LPS, viruses, oxLDL, and polarization cytokines (Fig. 7). Defective interaction with endothelium and angiogenesis-promoting matrix may be added to their anomalous relationship with the environment (Fig. 5).

Loss of nucleus-to-cytosol supply of menRNA or mascRNA: As both menRNA and mascRNA are continuously exported from nucleus to cytosol under normal conditions (Fig. 8), changes of the translational/ribosomal apparatus are likely to be linked to the complete loss of nucleus-to-cytosol supply of these tRNA-like molecules in the defective cells. Importantly, mascRNA displays very high steady-state levels within immune cells, while other cell types are essentially devoid of it, although they do express precursor *MALAT1* at normal levels [2,3]. While the exact molecular function of the high mascRNA levels in immune cells (Suppl. Fig. S1E) remains undefined in humans and other species carrying *MALAT1*-like genomic loci [62], key importance for immune homeostasis was highly likely by inference and is definitely confirmed by the present data. In this context, a recent study by Lu *et al.* [62] is of interest showing that mascRNA binds directly to multi-tRNA synthetase complex component glutaminyl-tRNA synthetase, and promotes global protein translation and cell proliferation by positively regulating QARS protein levels.

In the case of menRNA, on the other hand, steady-state levels in immune cells are very low. This may be entirely due, however, to the known CCACCA-tagging of menRNA for rapid degradation [63]. menRNA's primary nucleus-to-cytosol supply rate may be similar to that of mascRNA, which just remains stable as it is not CCACCA-tagged. ΔmenRNA cells display major disequilibrium at the tRNA/translational level with induction of initiation and elongation factors EIF3CL, EEF1A2 and CTIF, whereas translation initiation factor EIF1AY [18] was switched off. Further, there was deregulation of tRNAs, tRNA methyltransferases (TRMT61, TRMT2B), and RNA methyltransferase NSUN7.

Pioneering recent studies discovered hitherto unknown immune functions of tRNAs and their enzymatic processing products and may contribute to explain our current findings regarding the impact of menRNA and mascRNA ablation. tRNA products encompass tRNA-derived small RNAs (tsRNAs), tRNA-derived stress-induced RNAs (tiRNAs), and tRNA-derived fragments (tRFs). Pereira *et al.* [41] found that m(5)U54 tRNA hypomodification, from lack of methyltransferase TRMT2A, drives tsRNAs generation. As similar tRNA methyltransferases are deregulated in ΔmenRNA and ΔmascRNA cells, this may change tsRNA generation therein.

Yue *et al.* [42] found SLFN2 protection of tRNAs from stress-induced cleavage to be essential for T cell-mediated immunity. SLFN2 binds tRNAs and protects them from cleavage by the ribonuclease angiogenin (~12-fold induced in ΔmascRNA cells) [41]. SLFN2 deficient T cells display accumulation of stress-induced tiRNAs which inhibit translation and promote stress-granule formation. They found IL2R-β and IL2R-γ fail to be translationally up-regulated after T cell receptor stimulation, while we observed ~52-fold IL2R-β and ~13-fold IL2R-γ suppression in ΔmenRNA monocytes upon LPS stimulation. In these cells, SLFN family member SLFN12L was ~31-fold induced whereas SLNF5 was ~10-fold suppressed compared to controls. Yue *et al.* showed ROS trigger an oxidative stress response leading to translation repression which is countered by SLFN2. In ΔmenRNA monocytes we found LPS-stimulated ROS production as well as NOS2 expression are blunted, suggesting disturbance of a regulatory circuit encompassing menRNA, SLFN family members [26,64], and NO and ROS biosynthetic enzymes in these defective cells.

***Genetic variability of the NEAT1-MALAT1 genomic region in humans**:* Within a cohort of 7.492 individuals we found one rare (MAF 0.0113) *MALAT1* promotor SNP associated with low-level chronic inflammation. The current pilot study in a population wide-cohort was not designed to identify clinical phenotype associations with mascRNA or menRNA sequence variants which are known to occur, however, in humans. For five of the known menRNA SNPs MAFs are very low ranging from 0.0044 to 0.0002. Given the distinct functional sensitivity of the tRNA-like sequences to point mutations, it seems worthwhile to obtain full sequences in patient cohorts suffering from atherosclerosis and other disorders associated with chronic low-level inflammation.

***Conclusions and outlook**:* Beyond prior work in mice documenting immune function of the *NEAT1-MALAT1* region, the current study identifies menRNA and mascRNA as novel components of innate immunity with deep impact upon cytokine regulation, immune cell - endothelium interactions, angiogenesis, and macrophage formation and functions. These tRNA-like transcripts are prototypes of a new class of ncRNAs distinct from other small transcripts (miRNAs, siRNAs) by biosynthetic pathway and intracellular kinetics, suggesting a novel link for the apparent relevance of the

NEAT1-MALAT1 cluster in cardiovascular and neoplastic diseases. The *NEAT1-MALAT1* region has emerged as a highly integrated RNA processing circuitry. Its components MEN-β, MEN-ε, menRNA, *MALAT1*, *TALAM1*, and mascRNA are set for well-balanced interactions with each other, and ablation of any element leads to major cellular and systemic dysfunction. For future translational studies, our approach to study menRNA and mascRNA directly suggests new avenue since their highly dynamic levels may be more closely related to clinical parameters and clinical course than those of their nuclear precursors. They may also have value as therapeutic targets for pharmacological intervention since they are more easily accessible than their extremely complex nuclear-located precursor molecules.

Patients and Methods

For human studies approval was granted by the institutional ethics review board and the regulatory authorities. Investigation of human tissues was conform to the principles in the Declaration of Helsinki. Informed consent was given prior to inclusion of people in the study.

SHIP population study and cohorts

SHIP samples were genotyped using the *Affymetrix Genome-Wide Human SNP Array 6.0*. Genotyping of samples within SHIP-TREND was obtained in two batches using *Illumina Infinium HumanOmni2.5 BeadChip* and the *Illumina Infinium Global Screening Array*, respectively. Genotypes were determined using *Birdseed 2* for SHIP and the *GenomeStudio 2.0 Genotyping Module* (*GenCall algorithm*) for SHIP-TREND. Standard genotype quality control was performed excluding arrays < 92% sample call rate for SHIP and <94% sample call rate for SHIP-TREND and duplicates (based on estimated IBD), mismatches between reported and genotyped sex, genetic PCA outliers, and arrays with extreme heterozygosity. Variants with call rate < 0.95 and a Hardy-Weinberg equilibrium p-value < 0.0001 were removed before imputation. Pre-phasing and Imputation of genotypes was performed with the Eagle and Minimac3 software to HRC reference v1.1 panel on Michigan Imputation Server v1.0.1 (https://imputationserver.sph.umich.edu/). Further details regarding the SHIP cohorts are provided in the Supplement.

CRISPR-Cas9 experiments

THP-1 cells were grown in RPMI medium containing FCS (10% [v/v]) and penicillin/streptomycin (50 I.U./50 µg/ml). Parts of the menRNA and mascRNA regions were deleted from THP-1 cells using an adaptation of the CRISPR/Cas9 protocol described in Gundry *et al*. 2016. Protospacer sequences for each target gene were identified using the CRISPRscan scoring algorithm [www.crisprscan.org (Moreno-Mateos *et al.*)]. Extensive target searches employing http://www.crisprscan.com/, http://crispor.tefor.net/, and https://cctop.cos.uni-heidelberg.de identified no off-targets of potential relevance. DNA templates for single guide RNAs (sgRNAs) were generated by PCR (KAPA HiFi HotStart ReadyMix PCR Kit) using the pX458 plasmid containing the sgRNA scaffold sequence and using the following primers:

G1_human_mascRNA	taatacgactcactataGGTTGGCACTCCTGGTTTCCgttttagagctagaaatagc
G5_human_mascRNA	taatacgactcactataGGACGGGGTTCAAATCCCTGgttttagagctagaaatagc
G9_human_menRNA	taatacgactcactataGGGGCACGTCCAGCACGGCTgttttagagctagaaatagc
G10_human_menRNA	taatacgactcactataGGTCCAGCACGGCTGGGCCGgttttagagctagaaatagc
universal reverse	AGCACCGACTCGGTGCCACT

PCR products were used to generate sgRNAs by *in vitro* transcription using HiScribe T7 High Yield RNA Synthesis Kit. 0.5µg of purified sgRNA was incubated with Cas9 protein (1 µg; PNA Bio) for 15-20 min at room temperature. $2x10^5$ THP-1 cells were electroporated with the sgRNA/Cas9 complex using the Neon Transfection System at 1400 V, 20 ms, and one pulse. For the small RNA-deficient cell lines, two sgRNAs were selected at either end of the target sequence to delete the region in between. Deletion of *mascRNA* and *menRNA* was confirmed by PCR with the following primer pairs:

CRISPR_hu-masc_fw	CGTATTGTTTTCTCAGGTTTTGC
CRISPR_hu-masc_rev	ACCTCCCCAAAACTCCAAGA
CRISPR_hu-men_fw	TCTGTGAAAGAGTGAGCAGGA
CRISPR_hu-masc_rev	CCCAATGCTACCCCTCTAGG

Single-cell clones were generated by single-cell plating of the parental cell line. Gene deletions in the single-cell clones were confirmed by sequencing and proved to be stable over >25 passages so far.

Cell culture studies

Human monocyte cultures

Human THP-1 cells were cultured in RPMI 1640 medium with 10% fetal bovine serum, 2 mM L-glutamine, 100 U/mL penicillin and 100 µg/mL streptomycin. For gene expression analysis of wildtype (WT) and CRISPR-Cas9 targeted THP-1 cells under immune challenge, cells were stimulated with 100 ng/ml LPS, 10 ng/ml LPS 1 µg/ml, 1 ng/ml LPS, or 1 µg/ml Concanavalin A (Con A). After 24 h, RNA was isolated by TRIzol/Chloroform.

THP-1 monocyte adhesion to flow-primed human aortic endothelial cells

For analysis of WT and CRISPR-Cas9 targeted THP-1 monocytes adhesion to flow-primed endothelial cells, primary human aortic endothelial cells (HAECs) were cultured in Endothelial Growth Medium-2 with 10% fetal bovine serum, 100 U/mL penicillin and 100 µg/mL streptomycin and seeded to confluence in µ-Slide y-shaped ibiTreat chambers . Endothelial cells were exposed to unidirectional flow (20 dyn/cm^2) for 48 h using yellow/green perfusion sets prior to the experiment. THP-1 monocytes were labelled with 1,1'-dioctadecyl-3,3,3',3'-tetramethylindocarbocyanine (DiI) for 15 min at 37°C, respectively, and after three times wahsing 1×10^6 labelled cells were added to the flow reservoir for 30 min. After flow-termination, non-adherent cells were gently washed out with PBS, then cells were fixed with 4% paraformaldehyde and the number of cells adhering to both the straight and branched channel regions was assessed by fluorescence phase-contrast microscope quantified using ImageJ Software.

Tube formation angiogenesis assay

(a) Conditioned media transfer experiment: Tube formation by HAECs treated with ΔmenRNA and ΔmascRNA monocyte-conditioned media was assayed on reduced growth factor basement membrane extract (BME) in 96-well tissue cultured-treated clear-bottom plates (15×10^3 cells per well). Briefly, 60 µl of ice-cold BME was added per well and incubated at 37°C and 5% CO_2 for 30 min to allow gel formation. HAECs were plated on top of the gelled BME at a density of 1.5×10^4 cells/well in 50 µl culture medium followed by transfer of 50 µl of monocyte-conditioned media of both ΔmenRNA and ΔmascRNA and incubated further for 24 h. After tube formation was observed, endothelial cells were stained by adding 50 µl of 6 µM Calcein AM solution per well for 15 min at 37°C. Tubular network of the cells was captured using a fluorescent inverted microscope and quantified by ImageJ Software.

(b) Monocyte-HAEC co-cultures in matrigel: Endothelial tube formation in reduced growth factor matrigel was performed similarly as described above. Here, direct DiI-labeled co-cultured ΔmenRNA and ΔmascRNA monocytes at a cell density of 5×10^3 per well together with HAECs (1.5×10^4 cells/well) were added on the BME gel and cultured for 24 h at 37°C and 5% CO^2 to form tubular networks.

Reactive oxygen species assay

Intracellular ROS production in WT and CRISPR-Cas9 targeted THP-1 macrophages was determined as previously described using 2',7'-dichlorodihydrofluorescein diacetate (H2DCFDA). Upon cleavage of the acetate groups by intracellular esterases, the cell-permeant H_2DCFDA is retained within the cells and easily oxidized to the highly fluorescent 2',7'-dichlorofluorescin (DCF) in response to ROS production/oxidative stress. Control and CRISPR/Cas9-targeted THP-1 cells were cultured in black 96 wells (overnight treatment with 0,1 µM PMA) before LPS addition for 24h. After washing with HBSS, cells were incubated with 5 µM H2DCFDA (Molecular Probes) in HBSS for 1 h at 37 °C. Cells were washed again and ROS production was induced by 400 µM H_2O_2. Fluorescence intensity was quantified every 10 min (excitation 485 nm, emission 535 nm) at 37°C using a fluorescence plate reader (Tecan).

Cytokine measurements

Conditioned cell culture media of wildtype (WT) and CRISPR-Cas9 targeted THP-1 cells were tested for IFNγ, TNF, IL6, MCP1, IL10, and IL12p70 by use of *Mouse Inflammation Cytometric Bead Assay* (CBA) (*BD Biosciences, Heidelberg, Germany*) on a *FACS CantoII flow cytometer* (*BD Biosciences*) according to the manufacturer's protocol.

Cell proliferation studies

The proliferation assay of WT and CRISPR-Cas9 targeted THP-1 cells was conducted as follows: 5 x10^4 cells were seeded into clear 96 well plates, one plate for each time point. Proliferation was determined using WST1 reagent (*Sigma-Aldrich*) according to the manufacturer's instructions. Absorbance at 450 nm was measured 2 h after addition of WST1 and incubation at 37°C on a *Tecan* plate reader. Absorbance of WT cells was set to one at each time point.

Foam cell formation and oxLDL uptake

To induce foam cell formation, we seeded 5x10^5 THP-1 monocytes per well containing glass cover slips. Monocyte differentiation into macrophages was induced by adding 100 nM PMA to each well on days 0 and 1 and incubation for 48h hours. Thereafter the thus generated macrophages were washed with PBS, then incubated with 50µg/ml human ox-LDL for 24h in serum-free medium to induce foam cell formation. After ox-LDL incubation, Oil Red O staining (ORO) of the cells was performed as follows: wash with PBS, fix cells with 4% PFA/PBS for 15 min at RT, wash 3 times with PBS, rinse with 60% isopropanol for 15 s to facilitate the staining of neutral lipids, stain cells with filtered ORO working solution for 15 min at RT and in dark. ORO stock solution was prepared by dissolving 0.5 g ORO powder in 80 ml isopropanol (100%), mixed at 56 °C overnight, adjusted to 100 ml, mixed under gentle stirring, and filtered after pre-warming to 60°C. Working solution was prepared by diluting ORO stock solution with ddH2O 3:2 = factor 1.5. For staining, cells were rinsed with water and then hematoxylin used as a counterstain (cell nuclei) for 10 s. Destaining by washing with 60% isopropanol for 15 s, then PBS 3 times. Glass cover slips were taken out and mounted on slides for polarization microscopy and microphotography.

Monocyte-macrophage transition and macrophage polarization experiments

Monocyte-M0 macrophage differentiation and subsequent M1/M2 macrophage polarization studies employing FACS and TaqMan were conducted as follows: First, M0 macrophages were generated by incubation of THP-1 monocyte clones for seven days, with PMA at a concentration of 100 ng/ml. Thereafter, the cells were further incubated for another seven days, either with IFN-γ at 20 ng/ml plus LPS at 100 ng/ml to induce M1 polarization, or with IL-4 at 20 ng/ml plus IL-13 at 20 ng/ml to induce M2 polarization. The 'M0' TaqMan-based expression profiles and FACS data in Fig. 7 were obtained on day 7 of culture to characterize monocyte - M0 macrophage transition. The 'M1' and 'M2' expression profiles displayed there were obtained in day 14 of culture.

FACS analyses of the macrophage clones

After macrophage polarization, cells were washed once with ice-cold PBS and scrapped off using a mini scraper. Subsequently, macrophages were again washed with PBS + 5% FBS and incubated with 50 µl Fcγ-receptor block (*BD Biosciences*) in PBS for 10 min at RT to block unspecific binding. Cells were centrifuged at 300 x g for 5 min at 4°C. Then cells pellets were resuspended with 50 µl of FACS Buffer (PBS + 0,5%FBS + 0,05% NaN3) and stained with APC mouse anti-human CD14 (*BioLegend*), PE mouse anti-human CD11b (*BD Biosciences*) and Live/Dead Fixable Aqua Dead Cell Stain (*Invitrogen*) for 30 min at 4 °C in the dark. Cells were resuspended in 450 µl of FACS Buffer and analyzed with Attune™ NxT Flow Cytometer (*Thermo Fisher Scientific*). Statistical analysis was performed using GraphPad Prism 9 software. Experimental data were analyzed by using one-way analysis of variance (ANOVA) with Dunnett´s post hoc test for multiple comparisons. The distribution of variables was assessed by Kolmogorov–Smirnov tests of normality.

Human adenovirus and coxsackievirus B3 studies

THP-1 cells were cultured in *RPMI 1640* medium (ATCC modification + 10 % fetal calf serum + 1 % P/S) at 37 °C, 5 % CO2. $5x10^5$ cells were seeded in 12-well culture plates and differentiation to macrophage-like cells was triggered by addition of 0.1 μM PMA o/n. Afterwards cells were transduced with coxsackievirus B3 at MOI 30. Detection of CVB3 genome, replicative intermediates, and plaque forming units (PFU) was conducted as described. In the adenovirus experiments, cells were instead transduced with a recombinant adenoviral virus expressing GFP (AdV5-GFP) or an "empty" adenovector expressing no transgene, at MOI 25, 12h post PMA addition. Virus structures were described previously.

RNA sequencing and data analysis

For the transcriptome mapping of control *vs.* CRISPR-Cas9 generated ΔmenRNA or ΔmascRNA cells, four biological cell culture replicates were grown for each of the three clones. From each of these cultures separate total RNA isolations were conducted by *TRIZOL*/Chloroform method. Thereafter the individual RNA preps were pooled for each of the clones, and the three resulting RNA pools (control, ΔmenRNA, ΔmascRNA) were subsequently used for RNA-seq analyses as follows. RNA integrity was visualized using *Agilent Bioanalyzer 2100*. For NGS-library preparation we used *Illumina TruSeq Stranded Total RNA Library Prep* Human/Mouse/Rat (S45-S56) or *NEBNext Ultr II Directional RNA Library Prep* Kit Illumina (E7760S) in combination with the *NEBNext rRNA Depletion Kit* (Human/Mouse/Rat) (E6310L) (S145-S154). For all samples paired end (2x75bp) sequencing was carried out on an *Illumina NextSeq* platform using *NextSeq 500/550 High Output Kit v2.5* (150 cycles). The resulting reads were mapped to the human genome (GRCh37 release 87/hg19) using *STAR v2.7.5b* with standard options. We then ran the *htseq-count module* from software package *HTSeq* with the stranded=reverse option reflecting the used library kit. As we used rRNA-depleted samples, all with rRNA-annotation were excluded from further analyses. To detect differentially expressed genes we used the R package DESeq v1.34.1. Next we normalized the raw gene specific read counts as Transcripts per Million base pairs (TPM) in order to perform a gene set enrichment analysis (GSEA) using the *R package ssGSEA2.0* by mapping them against a selection of gene set collections from *Molecular Signature Database (MsigDB)*. We thus generated Enrichment Scores (ES) for each sample and various gene sets. ES reflects how strongly the majority of genes from an individual gene set are expressed per regarded sample. This ES was then normalized to account for variations in gene set size. To correct for multiple testing the ssGSEA package uses Benjamini-Hochberg method, which calculates false discovery rates (FDR). For any combination of gene set and sample with a FDR value ≥ 0.05 we set the NES to zero. The gene set collections we used were: C2.CP: Canonical pathways; KEGG selection as a subset of CP; C2.CGP: chemical and genetic perturbations; C7: immunologic signature gene sets.

Quantitative RT-PCR

cDNA transcription and qPCR were conducted using standard methods. Reference gene was HPRT. Expression levels measured by qPCR were quantified as $\Delta\Delta C_t$ values, determined by the C_t value of a candidate RNA minus the C_t of the reference gene. The TaqMan RT-PCR probes used are given in the Supplement.

Statistical analyses

Cell culture experiments: Statistical data analyses were done using *IBM SPSS Statistics 24* or *GraphPad* software. Descriptive statistics include absolute and relative frequencies for categorial variables and mean and standard deviation, median, and range for quantitative measurements. For inter-group comparisons Student's t-test or the χ^2 test was used for quantitative or categorical variables, respectively. P-values ≤ 0.05 are considered significant, and no Bonferroni adjustment has been performed.

Human molecular genetics: Genome-wide association analyses of healthy samples versus samples with inflammatory, metabolic, and/or cardiovascular conditions were performed via logistic regression analysis implemented in *snptest v2.5.2*. For sensitivity analysis samples were stratified by sex. Summary-level results were meta-analyzed with *METAL* (*Willer CJ, Li Y, Abecasis GR.*

METAL: fast and efficient meta- analysis of genomewide association scans. Bioinformatics. 2010;26:2190–1) using the classical approach which utilizes the effect size estimates and standard errors. Only variants with an imputation quality > 30% and Hardy-Weinberg equilibrium p-value > 0.0001 were included in the meta-analysis. Variants with p-value < 5×10^{-8} (the standard threshold) were considered to be genome-wide significant.

For further details on patients and methods please refer to the Supplement.

References

1. Gast, M.*, et al.* Long noncoding RNA NEAT1 modulates immune cell functions and is suppressed in early onset myocardial infarction patients. *Cardiovasc Res* **115**, 1886-1906 (2019).
2. Gast, M.*, et al.* Immune system-mediated atherosclerosis caused by deficiency of long non-coding RNA MALAT1 in ApoE-/- mice. *Cardiovasc Res* **115**, 302-314 (2019).
3. Gast, M.*, et al.* Long noncoding RNA MALAT1-derived mascRNA is involved in cardiovascular innate immunity. *J Mol Cell Biol* **8**, 178-181 (2016).
4. Cremer, S.*, et al.* Hematopoietic Deficiency of the Long Noncoding RNA MALAT1 Promotes Atherosclerosis and Plaque Inflammation. *Circulation* **139**, 1320-1334 (2019).
5. Lancellotti, P., Marechal, P., Donis, N. & Oury, C. Inflammation, cardiovascular disease, and cancer: a common link with far-reaching implications. *Eur Heart J* **40**, 3910-3912 (2019).
6. Poller, W.*, et al.* Non-coding RNAs in cardiovascular diseases: diagnostic and therapeutic perspectives. *Eur Heart J* **39**, 2704-2716 (2018).
7. Wilusz, J.E., Freier, S.M. & Spector, D.L. 3' end processing of a long nuclear-retained noncoding RNA yields a tRNA-like cytoplasmic RNA. *Cell* **135**, 919-932 (2008).
8. Kuhn, C.D., Wilusz, J.E., Zheng, Y., Beal, P.A. & Joshua-Tor, L. On-enzyme refolding permits small RNA and tRNA surveillance by the CCA-adding enzyme. *Cell* **160**, 644-658 (2015).
9. Pickar-Oliver, A. & Gersbach, C.A. The next generation of CRISPR-Cas technologies and applications. *Nat Rev Mol Cell Biol* **20**, 490-507 (2019).
10. Yuan, H.*, et al.* Pivotal role of NOD2 in inflammatory processes affecting atherosclerosis and periodontal bone loss. *Proc Natl Acad Sci U S A* **110**, E5059-5068 (2013).
11. Geirsson, A., Paliwal, I., Lynch, R.J., Bothwell, A.L. & Hammond, G.L. Class II transactivator promoter activity is suppressed through regulation by a trophoblast noncoding RNA. *Transplantation* **76**, 387-394 (2003).
12. Sundaram, B. & Kanneganti, T.D. Advances in Understanding Activation and Function of the NLRC4 Inflammasome. *Int J Mol Sci* **22**(2021).
13. Swanson, K.V., Deng, M. & Ting, J.P. The NLRP3 inflammasome: molecular activation and regulation to therapeutics. *Nat Rev Immunol* **19**, 477-489 (2019).
14. Schnappauf, O., Chae, J.J., Kastner, D.L. & Aksentijevich, I. The Pyrin Inflammasome in Health and Disease. *Front Immunol* **10**, 1745 (2019).
15. Sun, R., Hedl, M. & Abraham, C. Twist1 and Twist2 Induce Human Macrophage Memory upon Chronic Innate Receptor Treatment by HDAC-Mediated Deacetylation of Cytokine Promoters. *J Immunol* **202**, 3297-3308 (2019).
16. Bailey, C.C., Zhong, G., Huang, I.C. & Farzan, M. IFITM-Family Proteins: The Cell's First Line of Antiviral Defense. *Annu Rev Virol* **1**, 261-283 (2014).
17. Ignatova, V.V., Jansen, P., Baltissen, M.P., Vermeulen, M. & Schneider, R. The interactome of a family of potential methyltransferases in HeLa cells. *Sci Rep* **9**, 6584 (2019).
18. Godfrey, A.K.*, et al.* Quantitative analysis of Y-Chromosome gene expression across 36 human tissues. *Genome Res* **30**, 860-873 (2020).
19. Aguilo, F.*, et al.* Deposition of 5-Methylcytosine on Enhancer RNAs Enables the Coactivator Function of PGC-1alpha. *Cell Rep* **14**, 479-492 (2016).
20. Suzuki, T.*, et al.* Complete chemical structures of human mitochondrial tRNAs. *Nat Commun* **11**, 4269 (2020).
21. Van Haute, L.*, et al.* NSUN2 introduces 5-methylcytosines in mammalian mitochondrial tRNAs. *Nucleic Acids Res* **47**, 8720-8733 (2019).
22. Hunsucker, S.A., Spychala, J. & Mitchell, B.S. Human cytosolic 5'-nucleotidase I: characterization and role in nucleoside analog resistance. *J Biol Chem* **276**, 10498-10504 (2001).
23. Zhang, Q.*, et al.* The long noncoding RNA ROCKI regulates inflammatory gene expression. *EMBO J* **38**(2019).
24. Sadik, A.*, et al.* IL4I1 Is a Metabolic Immune Checkpoint that Activates the AHR and Promotes Tumor Progression. *Cell* **182**, 1252-1270 e1234 (2020).
25. Liu, X.*, et al.* Interleukin-4 Is Essential for Microglia/Macrophage M2 Polarization and Long-Term Recovery After Cerebral Ischemia. *Stroke* **47**, 498-504 (2016).
26. Kim, E.T.*, et al.* Comparative proteomics identifies Schlafen 5 (SLFN5) as a herpes simplex virus restriction factor that suppresses viral transcription. *Nat Microbiol* **6**, 234-245 (2021).
27. Arslan, A.D.*, et al.* Human SLFN5 is a transcriptional co-repressor of STAT1-mediated interferon responses and promotes the malignant phenotype in glioblastoma. *Oncogene* **36**, 6006-6019 (2017).
28. Fischietti, M.*, et al.* Schlafen 5 as a novel therapeutic target in pancreatic ductal adenocarcinoma. *Oncogene* **40**, 3273-3286 (2021).
29. Metzner, F.J., Huber, E., Hopfner, K.P. & Lammens, K. Structural and biochemical characterization of human Schlafen 5. *Nucleic Acids Res* **50**, 1147-1161 (2022).
30. Prabhudas, M.*, et al.* Standardizing scavenger receptor nomenclature. *J Immunol* **192**, 1997-2006 (2014).
31. Ley, K., Pramod, A.B., Croft, M., Ravichandran, K.S. & Ting, J.P. How Mouse Macrophages Sense What Is Going On. *Front Immunol* **7**, 204 (2016).
32. Wang, J. & Li, Y. CD36 tango in cancer: signaling pathways and functions. *Theranostics* **9**, 4893-4908 (2019).
33. Zhao, Y.*, et al.* The immunological function of CD52 and its targeting in organ transplantation. *Inflamm Res* **66**, 571-578 (2017).

34. Vitalle, J.*, et al.* The Expression and Function of CD300 Molecules in the Main Players of Allergic Responses: Mast Cells, Basophils and Eosinophils. *Int J Mol Sci* **21**(2020).
35. Vitalle, J., Terren, I., Orrantia, A., Zenarruzabeitia, O. & Borrego, F. CD300 receptor family in viral infections. *Eur J Immunol* **49**, 364-374 (2019).
36. Lewis Marffy, A.L. & McCarthy, A.J. Leukocyte Immunoglobulin-Like Receptors (LILRs) on Human Neutrophils: Modulators of Infection and Immunity. *Front Immunol* **11**, 857 (2020).
37. Griffiths, M.R., Botto, M., Morgan, B.P., Neal, J.W. & Gasque, P. CD93 regulates central nervous system inflammation in two mouse models of autoimmune encephalomyelitis. *Immunology* **155**, 346-355 (2018).
38. McCormack, R. & Podack, E.R. Perforin-2/Mpeg1 and other pore-forming proteins throughout evolution. *J Leukoc Biol* **98**, 761-768 (2015).
39. Mikulska, M.*, et al.* ESCMID Study Group for Infections in Compromised Hosts (ESGICH) Consensus Document on the safety of targeted and biological therapies: an infectious diseases perspective (Agents targeting lymphoid cells surface antigens [I]: CD19, CD20 and CD52). *Clin Microbiol Infect* **24 Suppl 2**, S71-S82 (2018).
40. Bassilana, F., Nash, M. & Ludwig, M.G. Adhesion G protein-coupled receptors: opportunities for drug discovery. *Nat Rev Drug Discov* **18**, 869-884 (2019).
41. Pereira, M.*, et al.* m(5)U54 tRNA Hypomodification by Lack of TRMT2A Drives the Generation of tRNA-Derived Small RNAs. *Int J Mol Sci* **22**(2021).
42. Yue, T.*, et al.* SLFN2 protection of tRNAs from stress-induced cleavage is essential for T cell-mediated immunity. *Science* **372**(2021).
43. Canton, J., Neculai, D. & Grinstein, S. Scavenger receptors in homeostasis and immunity. *Nat Rev Immunol* **13**, 621-634 (2013).
44. Nimmerjahn, F. & Ravetch, J.V. Fcgamma receptors as regulators of immune responses. *Nat Rev Immunol* **8**, 34-47 (2008).
45. Takai, T., Ono, M., Hikida, M., Ohmori, H. & Ravetch, J.V. Augmented humoral and anaphylactic responses in Fc gamma RII-deficient mice. *Nature* **379**, 346-349 (1996).
46. Sun, Y.*, et al.* Blockade of the CD93 pathway normalizes tumor vasculature to facilitate drug delivery and immunotherapy. *Sci Transl Med* **13**(2021).
47. Kielar, M.*, et al.* Soluble Complement Component 1q Receptor 1 (sCD93) Is Associated with Graft Function in Kidney Transplant Recipients. *Biomolecules* **11**(2021).
48. Tosi, G.M.*, et al.* CD93 as a Potential Target in Neovascular Age-Related Macular Degeneration. *J Cell Physiol* **232**, 1767-1773 (2017).
49. Oosting, M.*, et al.* Human TLR10 is an anti-inflammatory pattern-recognition receptor. *Proc Natl Acad Sci U S A* **111**, E4478-4484 (2014).
50. Pyonteck, S.M.*, et al.* CSF-1R inhibition alters macrophage polarization and blocks glioma progression. *Nat Med* **19**, 1264-1272 (2013).
51. Sjaarda, J.*, et al.* Blood CSF1 and CXCL12 as Causal Mediators of Coronary Artery Disease. *J Am Coll Cardiol* **72**, 300-310 (2018).
52. Gao, Y.*, et al.* LncRNA NEAT1 sponges miR-214 to regulate M2 macrophage polarization by regulation of B7-H3 in multiple myeloma. *Mol Immunol* **117**, 20-28 (2020).
53. Lino Cardenas, C.L.*, et al.* An HDAC9-MALAT1-BRG1 complex mediates smooth muscle dysfunction in thoracic aortic aneurysm. *Nat Commun* **9**, 1009 (2018).
54. Li, X., Ye, S. & Lu, Y. Long non-coding RNA NEAT1 overexpression associates with increased exacerbation risk, severity, and inflammation, as well as decreased lung function through the interaction with microRNA-124 in asthma. *J Clin Lab Anal* **34**, e23023 (2020).
55. Boros, F.A., Maszlag-Torok, R., Vecsei, L. & Klivenyi, P. Increased level of NEAT1 long non-coding RNA is detectable in peripheral blood cells of patients with Parkinson's disease. *Brain Res* **1730**, 146672 (2020).
56. Knutsen, E.*, et al.* The expression of the long NEAT1_2 isoform is associated with human epidermal growth factor receptor 2-positive breast cancers. *Sci Rep* **10**, 1277 (2020).
57. Apostolakis, S., Vogiatzi, K., Amanatidou, V. & Spandidos, D.A. Interleukin 8 and cardiovascular disease. *Cardiovasc Res* **84**, 353-360 (2009).
58. Velasquez, I.M.*, et al.* Association of interleukin 8 with myocardial infarction: results from the Stockholm Heart Epidemiology Program. *Int J Cardiol* **172**, 173-178 (2014).
59. Szomjak, E.*, et al.* Immunological parameters, including CXCL8 (IL-8) characterize cerebro- and cardiovascular events in patients with peripheral artery diseases. *Scand J Immunol* **71**, 283-291 (2010).
60. An, Z.*, et al.* Neutrophil extracellular traps induced by IL-8 aggravate atherosclerosis via activation NF-kappaB signaling in macrophages. *Cell Cycle* **18**, 2928-2938 (2019).
61. Gerszten, R.E.*, et al.* MCP-1 and IL-8 trigger firm adhesion of monocytes to vascular endothelium under flow conditions. *Nature* **398**, 718-723 (1999).
62. Lu, X.*, et al.* The tRNA-like small noncoding RNA mascRNA promotes global protein translation. *EMBO Rep* **21**, e49684 (2020).
63. Wilusz, J.E., Whipple, J.M., Phizicky, E.M. & Sharp, P.A. tRNAs marked with CCACCA are targeted for degradation. *Science* **334**, 817-821 (2011).
64. Puck, A.*, et al.* Expression and regulation of Schlafen (SLFN) family members in primary human monocytes, monocyte-derived dendritic cells and T cells. *Results Immunol* **5**, 23-32 (2015).
65. Geirsson, A., Bothwell, A.L. & Hammond, G.L. Inhibition of alloresponse by a human trophoblast non-coding RNA suppressing class II transactivator promoter III and major histocompatibility class II expression in murine B-lymphocytes. *J Heart Lung Transplant* **23**, 1077-1081 (2004).

66. Kawase, T.*, et al.* p53 target gene AEN is a nuclear exonuclease required for p53-dependent apoptosis. *Oncogene* **27**, 3797-3810 (2008).
67. Roberts, O. & Paraoan, L. PERP-ing into diverse mechanisms of cancer pathogenesis: Regulation and role of the p53/p63 effector PERP. *Biochim Biophys Acta Rev Cancer* **1874**, 188393 (2020).
68. Cruikshank, W.W., Kornfeld, H. & Center, D.M. Interleukin-16. *J Leukoc Biol* **67**, 757-766 (2000).
69. Wang, Z.*, et al.* CD146, from a melanoma cell adhesion molecule to a signaling receptor. *Signal Transduct Target Ther* **5**, 148 (2020).
70. Kraler, S.*, et al.* Soluble lectin-like oxidized low-density lipoprotein receptor-1 predicts premature death in acute coronary syndromes. *Eur Heart J* (2022).

For the complete set of references please refer to the Supplement.

Acknowledgements

M.G., V.N., X.W., A.H. and W.P. conducted and analyzed the cell biological and molecular genetic studies. M.G., L.H.M., X.W., A.T., A.W.K. and W.P. designed, conducted and evaluated the CRISPR-Cas experiments. A.W.K., A.T. and S.W. supervised and analyzed the RNA-sequencing experiments and their statistical analysis. B.R., S.W. and A.W.K. conducted multivariate statistical analyses of the SNP data from the SHIP study cohorts. H.V., W.H., U.V., S.F. and M.D. are coordinators of the SHIP trials program. A.B., K.K. and X.W. conducted and evaluated the virological experiments. S.S., T.Z., C.S., and B.H. provided logistic and organizational support. T.H. and S.N. generated the NEAT1 and MALAT1 knockout mice and made critical intellectual input regarding the molecular pathology of the CRISPR-generated clones. F.S. and W.C.P. were critically involved in interpretation of the cytokine, cell-cell interaction and angiogenetic data. W.P. and A.H. initially designed and supervised the project, and drafted and finalized the manuscript based on input from the other authors. W.P. and T.Z. received grants B19-006_SE (FKZ 81X2100257 and =81X2710170 'Transcriptome analysis of circulating immune cells to improve the assessment of prognosis and the response to novel anti-inflammatory treatments after myocardial infarction') and B18-004_SE (FKZ 81X2100253, 'Functional role and therapeutic potential of the long noncoding RNA *NEAT1-MALAT1* genomic region in cardiovascular inflammation control and atheropathogenesis') from the German Center for Cardiovascular Research (DZHK). TZ is supported by the German Center of Cardiovascular Disease (FKZ 81Z0710102; Systems-medicine approaches in cardiovascular disease, partner site project). A.H. received a grant (FKZ 01ZX1906B 'Systems-medicine of pneumonia-aggravated atherosclerosis') from the German Federal Ministry of Education and Research (BMBF). A.H. is supported by the Berlin Institute of Health (BIH) Advanced Clinician Scientist program.

Figure Legends

Figure 1

Targeted deletion of tRNA-like transcripts from the NEAT1-MALAT1 cluster

Panel A: The *NEAT1-MALAT1* gene cluster encodes two primary transcripts which are subsequently processed to transcripts of vastly different size. The *NEAT1* locus yields the 23kb MENβ (NEAT1_1) and 3.7kb MENε (NEAT1_2). Of note, the long MENβ transcript forms an unusual triple helix structure at its 3'-end which has been shown to stabilize this long transcript. From the primary transcript, an additional short tRNA-like 59nt 'menRNA' is generated through RNAse P and Z enzymatic cleavage.

Panel B: The *MALAT1* locus yields a 8.3 kb primary transcript also forms a stabilizing triple helix at the 3'-end, and through enzymatic cleavage another small tRNA-like 59nt 'mascRNA'. Using CRISPR-Cas9, we developed human monocyte-macrophage cell lines with menRNA or mascRNA sequence deletions as indicated. The editing procedures occur outside of the primary transcript sequences required for regular formation of the triple-helix structures at their 3'-ends which support stabilization of the respective lncRNAs. Under the experimental conditions employed there was no change in *NEAT1* expression as detectable by RNA-sequencing (RNA-seq) and qRT-PCR.

For a high resolution version of this figure please refer to the Supplement. Further details regarding the targeted genomic regions (Suppl. Fig. S1AB), recombinant expression and Northern blot analysis of menRNA (Suppl. Fig. S1CD), structure prediction for residual transcripts (Suppl. Fig. S2), *in vitro* transcription of single-guide RNAs for CRISPR-Cas9 experiments (Suppl. Fig. S3A), and PCR analysis and sequencing of the deletion clones (Suppl. Fig. S3BC) are provided in the Supplement.

Figure 2

Gene set enrichment analysis of ΔmenRNA and ΔmascRNA monocytes

RNA-seq identified profound alterations in the baseline transcriptomes of ΔmenRNA *(panel A)* and ΔmascRNA *(panel B)* monocytes. Depicted is a gene set enrichment analysis (GSEA) of the RNA-seq datasets, mapped against gene sets from the Molecular Signature Database's (MSigDB) collection derived from the Kyoto Encyclopedia of Genes and Genomes (KEGG) pathway database. For a high resolution version of this figure please refer to the Supplement. Further details regarding the RNA-seq analyses are provided in Suppl. Tables S1/S2.

Figure 3

Disturbances of innate immune sensing, transcription and translation in defective monocytes

Panels A-E (Innate immune sensing)

A key finding of the RNA-seq was imbalance between multiple innate immune sensors in ΔmenRNA cells under baseline *(panel A)* and LPS-stimulated *(panel B)* conditions (Table S1A). Amongst cytosolic receptors, NOD2 [10] was ~8-fold and CIITA [65] ~17-fold induced, whereas NLR-class receptors NLRC3, NLRC4, NAIP and MEFV [12] were suppressed in ΔmenRNA monocytes. Amongst membrane-bound Toll-like receptors, TLR 2 showed ~10-fold elevated baseline expression in ΔmenRNA cells. In contrast, defective induction was seen for TLR6, TLR1, TLR8, TLR10, and TLR7 in ΔmenRNA upon LPS challenge *(panel B)*. In the context of the observed massive baseline induction of NOD2 and TLR2 it is notable that twist family bHLH transcription factor 2 (TWIST2) [15] was ~10-fold down in these ΔmenRNA cells *(panels GH)*, and that loss of NLRC3 and TWIST2 expression in ΔmenRNA monocytes could not be rescued by LPS *(panel E,* compare Fig. 6A for related findings in macrophages). mascRNA cells likewise displayed anomalies in immune sensor expression *(panel C)*(Table S2A), however different from those observed in ΔmenRNA cells. Prominent in ΔmascRNA monocytes was the induction of interferon (IFN)-induced transmembrane (IFITM) proteins which represent primary cellular defenses against multiple viruses [16]. Upon PMA-induced differentiation of ΔmenRNA and ΔmascRNA monocytes into macrophages multiple further baseline anomalies of antiviral defense genes became apparent (Suppl. Fig. S9).

In both defective clones there was imbalance of apoptosis-related genes. In LPS-stimulated ΔmenRNA cells *(panel B)* apoptosis regulator BOK and Niban apoptosis regulator FAM129C were upregulated, whereas serine/threonine kinase RIPK3 and apoptosis inhibitor NAIP and CARD14 were suppressed here. In ΔmascRNA cells *(panel C)*, NAIP was induced while apoptosis enhancing nuclease AEN [66] was ~ 3.-fold and p53 apoptosis effector PERP [67] ~ 5.1-fold suppressed (Table S2A).

In addition to alterations of protein-coding genes, RNA-seq identified deregulation of long noncoding RNAs (lncRNAs) and antisense (AS) RNAs in ΔmenRNA and ΔmascRNA monocytes (Tables S1D/2D). Thus, ΔmenRNA cells showed ~7-fold downregulation of a recently discovered novel transcript designated 'MARCKS cis-regulating lncRNA promoter of cytokines and inflammation' or 'regulator of cytokines and inflammation' (ROCKI) (*see Fig. 4DE*)(Tables S1D/S2D). This transcript of particular interest was identified by Zhang *et al.* [23] conducting a genome-wide scan of TLR-stimulated macrophages for pairs of cis-acting lncRNAs and protein-coding genes involved in innate immunity.

Panels F-I (Transcriptional level)

Several transcription factors (TF), nuclear factors and epigenome modifiers were deregulated in defective cells. At the transcriptional level, in addition to TWIST2, TF GATA2 was ~4-fold induced and GATA6 ~20-fold suppressed, and NFATC2 switched off in ΔmenRNA cells *(panels GH)* at baseline already (compare Fig. 5AD for related findings in macrophages). Further TFs (SOX4, ETS1, STAST4) and epigenome modifiers turned into disequilibrium upon LPS challenge, among them histone deacetylases (HDAC4, HDAC9, HDAC11), lysine demethylases (KDM1B, KDM7A), and METTL methyltransferase family members [17] known or predicted to methylate DNA, RNA or proteins (METTL7A, METTL7B). *Panel D* summarizes the most prominent changes of cytosolic and membrane-bound innate immune sensors, and of transcription factors and epigenome modifiers, in ΔmenRNA and ΔmascRNA monocytes. *Panel E* exemplifies how LPS-stimulation exacerbates several of these deregulations (e.g. CIITA and NOD2) while this stimulation it is uncapable to overcome certain blocks (e.g. of NLRC3 or TWIST2)(see Fig. 6A for related findings in macrophages). Bar graphs show means ± SE from three biological replicates.

Panels K-N (Translational level)

Particular anomalies were identified regarding translation factors, ribosomal proteins and nucleic acid modifiers in ΔmenRNA *(panels KL)* as well as ΔmascRNA monocytes *(panel M)*. In ΔmenRNA cells the translation initiation and elongation factors EIF3CL, EEF1A2, and CTIF were induced, whereas the initiation factor EIF1AY was completely silenced [18]. DEAD-box helicase DDX3Y and ribosomal protein RPS4Y1 were switched off, too, in menRNA-deficient cells under baseline conditions *(panel K)* and these shutdowns persisted upon LPS stimulation of the cells *(panels L)*. By contrast, RNA methyltransferase NSUN7 which is able to reinforce transcription concomitant with m(5)C marks on enhancer RNAs [19,21], was switched on in ΔmenRNA monocytes *(panel K)* while undetectable in control cells. At the level of tRNAs, genomically or mitochondrially encoded tRNAs [20,21] and tRNA methyltransferases (TRMT61A, TRMT2B) displayed major deregulation in ΔmenRNA cells *(panel KL)*. ΔmascRNA cells *(panel M)*, on the other hand, showed none of these alterations, whereas cytosolic nucleotidase NT5C1A [22] which dephosphorylates the 5' and 2'(3')-phosphates of deoxyribonucleotides and has broad substrate specificity, is ~10-fold suppressed here.

Panel N summarizes major changes regarding the translational machinery in menRNA-deficient monocytes, including translation factors and a poly(A) binding protein, tRNA methylases, two SLFN family members, angiogenin (ANG), and IL2 receptor subunits β and γ. These alterations within the translation system of ΔmenRNA monocytes may lead to accumulation of anomalous tRNAs and tRNA fragments (tiRNAs, tsRNAs), in particular under conditions of cellular or immune stress (for details see the discussion section *Loss of nucleus-to-cytosol supply of menRNA or mascRNA*).

Figure 4

menRNA and mascRNA deletion results in loss of cytokine control and imbalance of interleukin systems

Panel A: Prominent was massively elevated expression and secretion of the IL-8, TNF, and IL1B in unstimulated ΔmenRNA cells. Cytometric bead assay protein data on media conditioned by control monocytes (green), ΔmenRNA (orange), and ΔmascRNA cells (red). *Panel B*: qRT-PCR quantification of gene expression levels. For all three proinflammatory cytokines, ΔmenRNA displayed far more pronounced induction than ΔmascRNA cells. *Panel C*: ΔmascRNA monocytes displayed exaggerated induction of IL1A, IL1B, IL10, and ISG15 expression upon LPS-stimulation as compared to controls. Only stimulated ΔmenRNA cells showed a further increase of IL8 expression, whereas IL16 [68] was suppressed in this clone at baseline, and failed to become induced upon LPS challenge.

Panels D-F: RNA-seq identified further anomalies of IL and TNF systems. Among receptors, IL4R was ~7-fold and IL4-induced gene (IL4I1) ~11-fold suppressed in stimulated ΔmenRNA cells *(panels DE)*. Even more pronounced was disequilibrium in the IL18 system (IL18R1 >70-fold inhibited, IL18 receptor accessory protein IL18RAP switched off). In the IL2 system, receptor subunit IL2R-β was ~52-fold and IL2R-γ ~13-fold suppressed in LPS-stimulated ΔmenRNA monocytes (*panel E*). Regarding the IL1 system, IL1 receptor antagonist IL1RN was ~12-fold and IL1 receptor associated kinase IRAK2 ~8-fold down in ΔmenRNA cells. Among the ligands, IL16 expression remained ~18-fold blunted even upon LPS-challenge (compare *panel C*).

Figure 5

Impact of menRNA and mascRNA deletions upon monocyte-endothelium interactions and angiogenesis

For a high resolution version of this figure please refer to the Supplement.

Panels A-D (Endothelial cell interactions)

At the cellular level, ΔmenRNA monocytes displayed an anomalous growth pattern with spontaneous cell cluster formation in liquid culture *(panel A)*. Despite this morphological anomaly, there was no significant difference in their cell proliferation kinetics compared to ΔmascRNA and control monocytes (data not shown). ΔmenRNA cell showed defective endothelial adhesion under multiple flow conditions *(panel B)*. While expression of vascular cell adhesion molecule 1 (VCAM-1) was ~200-fold induced by LPS, starting from a very low baseline level in control cells, this induction was almost entirely blunted in ΔmenRNA cells. Similarly, the LPS-dependent induction of ICAM1 was strongly reduced in these defective cells *(panel C)*. Transfer of ΔmenRNA monocyte-conditioned medium to HAEC endothelial monolayers triggered changes in the expression of multiple genes including ~10-fold increased ISG15, ~8-fold increased IL8, ~7-fold increased IRAK1, ~7-fold increased ICAM1, whereas ΔmascRNA-conditioned medium exerted no such influence. Bars graphs show means ± SE from two biological replicates *(panel D)*.

Panels E-G (Cell adhesion molecule profiles)

RNA-seq identified profound deregulation of multiple cell adhesion molecules in ΔmenRNA cells *(panels EF)* including adhesion G protein-coupled receptors (GPRs, BAIs) [40], intercellular adhesion molecules (ICAMs), neural cell adhesion molecules (NCAMs), integrins (α_M, α_L, α_X, α_1, α_4, α_6, β_7), vascular cell adhesion molecule (VCAM1), and ESAM (endothelial cell-specific adhesion molecule).

ΔmascRNA cells *(panel G)* displayed deregulation of several cell adhesion molecules, too, however distinct from those observed in ΔmenRNA cells. Thus, neuronal growth regulator NEGR1, involved in neuronal growth and connectivity and cell-cell interactions in general, is ~28-fold down in Δmen19 while unaltered in Δmasc19 cells. Cytoskeleton regulating NCKAP1 was ~14-fold increased in ΔmascRNA while unaltered in ΔmenRNA cells.

Panels H-M (Angiogenesis, growth factors and chemokine systems)

Quantitative effects of both ΔmenRNA (orange) and ΔmascRNA (red) monocyte-conditioned media upon HAEC-based tube formation in an angiogenesis assay, as compared to Cas9 controls (green). Supernatant from each of the defective cell clones highly significantly reduced the number of tubes formed. Bars graphs show means ± SE from three biological replicates *(panel H).* Beyond a quantitative effect of secreted factors from the cells, direct co-culture of ΔmenRNA as well as of ΔmascRNA monocytes with the HAECs lead to profound alterations of HAEC cell morphology. In co-cultures with any of the defective monocytic clones, there was a massive increase in the size of HAECs at many branch side nodes where ≥3 endothelial cells came into contact (white arrows in the upper and middle rows). When the defective monocytes clones were red-stained (with DiI) before addition to the HAEC-matrigel mixture, there was significant accumulation of red cells (black arrows in the lower row) at branch side nodes where HAEC hypertrophy occurred *(panel I).*

Multiple growth and angiogenesis-associated factors as well as chemokines were in disequilibrium in both ΔmenRNA *(panels KL, table S1G)* and ΔmascRNA monocytes *(panel M, table S2G)*. Compared to controls, ΔmascRNA monocytes showed ~12-fold increased baseline expression of angiogenin (ANG), a key protein of angiogenesis interacting with endothelial and smooth muscle cells resulting in cell migration, invasion, proliferation and formation of tubular structures. Beyond these properties, ANG exhibits ribonucleolytic activity critical for its biological functions and is also involved in nucleic acid metabolism. ΔmascRNA cells *(panel M)* displayed induction of angiopoietins ANGPT1 and ANGPT4, angiopoietin-like 4 (ANGPTL4), and vascular endothelial growth factor (VEGFA). While ΔmenRNA monocytes likewise showed induction of VEGFA, angiopoietin like 6 (ANGPTL6) was ~7-fold down and ANGPT1 shut off here.

Within the transforming growth factor system, TGF β2 (TGFB2) expression was undetectable in controls but strongly induced in ΔmenRNA cells *(panels KL)*. Similarly, one latent TGF β-binding protein (LTBP1) and TGFBR3L were induced from low baseline levels. Conversely, TGF β3 (TGFB3) was downregulated as well as the TGF β-induced gene TGFBI. GREB1, a suppressor of TGF-β signaling, was undetectable in controls, but high in ΔmenRNA cells. ΔmascRNA monocytes *(panel M)* also displayed significant TGF system deregulation, but distinct from ΔmenRNA cells. Thus, TGF α (TGFA) was ~8-fold induced in ΔmascRNA cells while TGF β2 expression was unchanged. Another latent TGF β-binding protein (LTBP2) and TGF β induced (TGFBI) gene were upregulated here. Insulin like growth factor (IGF) system is likewise disturbed, and growth differentiation factors including GDF5, a bone morphogenetic protein (BMP) ligand from the TGF-β superfamily.

While two chemokine receptors (CXCR4 and CCR2) were ~3-fold induced in stimulated ΔmenRNA cells *(panels KL)*, C-X3-C chemokine receptor 1 (CX3CR1) (fractalkine receptor) displays ~9-fold reduced expression. Receptors CCR7 and

CXCR3 were massively ~44-fold suppressed in ΔmenRNA cells. Among ligands, CXC-type CXCL10, CXCL11, CXCL13, and CXCl16 displayed up to ~10-fold suppressed expression in this clone.

Figure 6

Antiviral response, foam cell formation and oxLDL uptake of ΔmenRNA and ΔmascRNA macrophages

For a high resolution version of this figure please refer to the Supplement.

Panels A-D (Response to human-pathogenic viruses)

PMA-induced differentiation of ΔmenRNA cells to adherent macrophages rendered the cells susceptible to efficient transduction by recombinant viruses derived from the human-pathogenic double-stranded DNA (dsDNA) adenovirus type 5. At a multiplicity of infection (MOI) 25, the GFP-expressing virus AdV-CMV-GFP efficiently transduced these macrophages, resulting in strong GFP expression in >50 % of cells (Suppl. Fig. S8A). In thus generated macrophages, without LPS stimulation or virus exposure, the IL8 expression level was massively ~130-fold compared to controls (*panel A*). Transduction with a recombinant adenovirus without the GFP expression cassette (AdV-RR5) resulted in a significant decrease of IL8 expression level in these ΔmenRNA cells, to ~40-fold of the level in control macrophages. In contrast, control cells displayed no change of their very low baseline IL8 expression, in response to AdV-RR5. ΔmenRNA macrophages showed ~17-fold higher baseline TNF expression compared to controls. Transduction with AdV-RR5 resulted in no significant change of TNF transcription, neither in ΔmenRNA nor control cells. Similarly, TLR2 expression was ~5-fold higher in ΔmenRNA macrophages vs. controls, without changes in response to AdV-RR5. Several other genes were induced in response to transduction (RIG-like receptors RLR1 and RLR2, ISG 15), but without significant differences between defective and control cells. Striking was a complete shutdown of several genes already suppressed in ΔmenRNA monocytes (Fig. 3A-E, Fig. 4EF) before their transformation into macrophages: NOD-like innate immune genes NLRC3 and MEFV, IL2 receptor subunits β and γ, transcription factor TWIST2, and NFATC2. None of these genes fully silenced in macrophages could be 'rescued' by adenovirus exposure, similar to findings in LPS-stimulated monocytes (Fig. 3A-E, Fig. 4EF). Bar graphs show means ± SE from three biological replicates.

Panel B shows the response of ΔmenRNA macrophages to Coxsackievirus B3, an important human-pathogenic single-stranded RNA (ssRNA) virus. Their IL8 response to CVB3 (~5-fold induction upon virus exposure) was opposite to that to AdV-RR5 (reduction of IL8 to ~2/3 of the high baseline level). Efficient transduction by CVB3 was detected by qRT-PCR, while CVB3 (-) minus strand-specific RT-PCR indicative of active replication was negative for all clones (Suppl. Fig. S8B). Bar graphs show means ± SE from two biological replicates. *Panel C* displays blunted NOS2 expression (qRT-PCR) by ΔmenRNA but not ΔmascRNA macrophages at baseline and upon adenovirus exposure, as well as impaired ROS production after LPS or H_2O_2 challenge. Bars graphs show means ± SE from three biological replicates. *Panel D* summarizes the leading anomalies in CRISPR-Cas9 modified human ΔmenRNA macrophages.

Panels E-K (Foam cell formation and oxLDL uptake)

Panels E-G: Whereas ΔmascRNA macrophages displayed an oxLDL uptake pattern undistinguishable from that of control cells (intracellular Oil Red-positive OR^+ vesicles as indicated by red arrows). In contrast, essentially no normal-sized intracellular OR^+ vesicles were observed in ΔmenRNA macrophages ($p< 0.0001$) 24 hrs after oxLDL exposure. A minor number of very small OR^+ particles is visible in ΔmenRNA cells. It appears these minute particles are not artifacts, and do not represent spontaneous intracellular accumulation of any OR^+ material in the ΔmenRNA cells, but residues of defective oxLDL endocytosis since they do not show up without prior oxLDL challenge (*panel G*). For high resolution microphotographs please refer to the figure's source file. The striking defect of oxLDL uptake by ΔmenRNA macrophages is paralleled by loss of scavenger receptors CD36, MCAM (CD146)[69], MSR1, and OLR1 (LOX1) [70] (*panel F*). Bars graphs show means ± SE from four biological replicates.

Panels H-K: These changes occur in the context of further anomalies, identified by RNA-seq of monocytes, affecting phagocytosis as an evolutionarily conserved general defense mechanism involving, beyond scavenger receptors, Fcγ receptors (FcγRs) [44,45] and complement receptors (CRs). FCGR2 genes encoding Fc fragments of inhibitory FcγRIIB are suppressed in ΔmenRNA cells and not rescuable by LPS (*panel HI*). Complement component properdin (CFP) is likewise down. Of note, ΔmascRNA cells (*panel K*) display opposed deregulation of the same FCGR2 genes, and induction of properdin and other complement components. Remarkable is also strong opposed deregulation of CD93 in ΔmenRNA compared to ΔmascRNA monocytes. While massively induced in ΔmenRNA cells, CD93 was shut down in ΔmascRNA monocytes, contrasting with robust expression in controls. CD93 is a lectin receptor involved in control of the immune response [37]. Another distinction between the defective clones regards MPEG-1 (perforin-2), an evolutionary ancient protein involved in the unspecific immune defense [38], which was ~16-fold down in ΔmenRNA while upregulated in ΔmascRNA cells.

Scavenger receptor CD36 [30,32] was ~48-fold down in ΔmenRNA monocytes. They also show suppression of Cluster of Differentiation (CD) marker CD40, a member of the TNF receptor family, and of CD52, a glycoprotein modulating T-cell activation. CD300A and CD300C, involved in viral immune evasion, were ~26-fold and ~5-fold suppressed, respectively. None of the group 1 CD1 molecules, normally expressed on cells specialized in antigen presentation, could be induced by LPS-treatment of ΔmenRNA cells. Finally, leukocyte immunoglobulin like receptors (LILRs) were broadly deregulated. ΔmascRNA cells *(panel K)* displayed none of these ΔmenRNA-associated CD molecule or LILR deregulations.

Figure 7

Anomalous monocyte-macrophage differentiation and polarization

For a high resolution version of this figure please refer to the Supplement.

Whereas the monocyte clones had similar proliferation kinetics in liquid culture (Fig. 5A), they differed with respect to their macrophage differentiation and response to polarization agents. Monocyte-M0 macrophage differentiation and subsequent M1/M2 macrophage polarization were conducted as follows: First, M0 macrophages were generated by incubation of THP-1 monocyte clones for seven days, with PMA at a concentration of 100 ng/ml. Thereafter, the cells were further incubated for another seven days, either with IFN-γ at 20 ng/ml plus LPS at 100 ng/ml to induce M1 polarization, or with IL-4 at 20 ng/ml plus IL-13 at 20 ng/ml to induce M2 polarization. 'M0' expression profiles and FACS data in panels A-C were obtained on day 7 of culture. The 'M1' and 'M2' expression profiles in panels BC were obtained on day 14 of culture. Expression profiling allowed unequivocal distinction between each of the three clones (ΔmenRNA, ΔmascRNA, controls).

Panel A: ΔmenRNA monocytes were uncapable of normal differentiation into M0 macrophages upon PMA exposure, consistent with the grave disturbance of CD molecule expression in these monocytes (including CD11b, CD11c). In accordance with these transcription level alterations, FACS analysis identified defective transition from monocytes (both ΔmenRNA and ΔmascRNA) to M0 macrophages as assessed by CD11b and CD14 expression. The graphs display the statistics of 5-6 independent biological samples (one-way ANOVA multiple comparisons, FACS gatings in Suppl. Fig. S9B).

Panel B: A distinctive expression profile was characteristic of ΔmenRNA cells. It was previously observed in ΔmenRNA monocytes (Fig. 4A-C), ΔmenRNA M0 macrophages, and preserved upon their treatment with M1 or M2 polarization protocol. This conserved pattern encompasses IL1B, CD93, TGFB2, CSF1 and its receptor CSF1R. While high pro-inflammatory IL1B expression is common to M1-polarized cells, the massive induction of CD93 or the CSF1 - CSF1 receptor system [51] observed here is not commonly associated with either M1 or M2 polarized cells. Bars graphs in panels B and C show means ± SE from four biological replicates. The expression levels of each gene are normalized to the control clone level at the respective time, i.e. day 7 for M0 macrophages, and day 14 for M1 and M2 polarized cells.

Panel C: Beyond M0 differentiation, another characteristic expression profile developed for ΔmascRNA cells. A "M2-prone" pattern comprising CD163^{hi} CD200R1^{hi} CD206^{hi} CX3CR1^{hi} TLR10^{hi} was observed in ΔmascRNA macrophages upon the M2 polarization protocol. This is easily distinguished from the profile of control and ΔmenRNA cells after this treatment. TLR10 was recently identified as anti-inflammatory pattern-recognition receptor [49] and added to this "M2-prone" pattern.

Panel D: At the end of the 14 days M2 polarization protocol, the morphological aspect of M2-polarized ΔmenRNA macrophages was grossly different from that of control cells and ΔmascRNA cells. At that time, "colony-like" cell clusters became visible in both control and ΔmascRNA cultures, whereas the distribution of the M2-polarized ΔmenRNA macrophage remained essentially homogeneous. For high resolution microphotographs please refer to the Supplement.

Figure 8

Summary figure and working model

Analysis of monocytes-macrophages carrying narrowly targeted deletions of the novel tRNA-like molecules indicates they are critical building blocks required for balanced function of innate immunity. The grave disturbance of multiple immune sensor systems - with complex downstream sequelae – might be addressed by a working hypothesis invoking a primordial defect linked to the peculiar structure of menRNA and mascRNA. They closely resemble common tRNAs, strongly suggesting that they also interact with the ribosomal machinery. Accordingly, ablation of nucleus-to-cytosol supply of menRNA or mascRNA would cause imbalance within the translation system, consistent with the observed

deregulation of multiple translation factors, tRNAs, tiRNAs, and ribosomal proteins in defective cells. Delineation of a specific molecular mechanism to prove this hypothesis is far beyond the scope of this study which attempted to first identify any distinct biological functions of menRNA and mascRNA within the *NEAT1-MALAT1* cluster.

Considering the minute and narrowly targeted genetic interventions employed, the extent of disturbances from key innate immune sensors to complex downstream sequelae, is unexpected. Beyond primary defects at sensor level, the grave loss of cytokine control, angiogenesis-modifying effects of ΔmenRNA and ΔmascRNA monocytes, and defects of key ΔmenRNA and ΔmascRNA macrophage functions, constitute the first known biological functionalities of these cytosolic molecules. From this starting point it appears warranted to generate murine models, with cell type-specific inducible knockout of menRNA or mascRNA only, to further elucidate their functions in disease models.

For future translational studies, our approach to study menRNA and mascRNA directly suggests new avenue since their highly dynamic levels may be more closely related to clinical parameters and clinical course than those of their nuclear precursors. They may also have value as therapeutic targets for pharmacological intervention since they are more easily accessible than their extremely complex nuclear-located precursor molecules. A prior observation that recombinant mascRNA [3] abolishes virus replication in cardiomyocytes does suggest potential of mascRNA- and menRNA-targeting interventions.

From an evolutionary perspective, the *NEAT1-MALAT1* genomic region appears as a highly integrated RNA processing circuitry critically contributing to immune homeostasis. Its components MEN-β, MEN-ε, menRNA, *MALAT1*, *TALAM1*, and mascRNA are obviously set for well-balanced interactions with each other. Genetic ablation of any element therefore leads to major dysfunction.

Figures

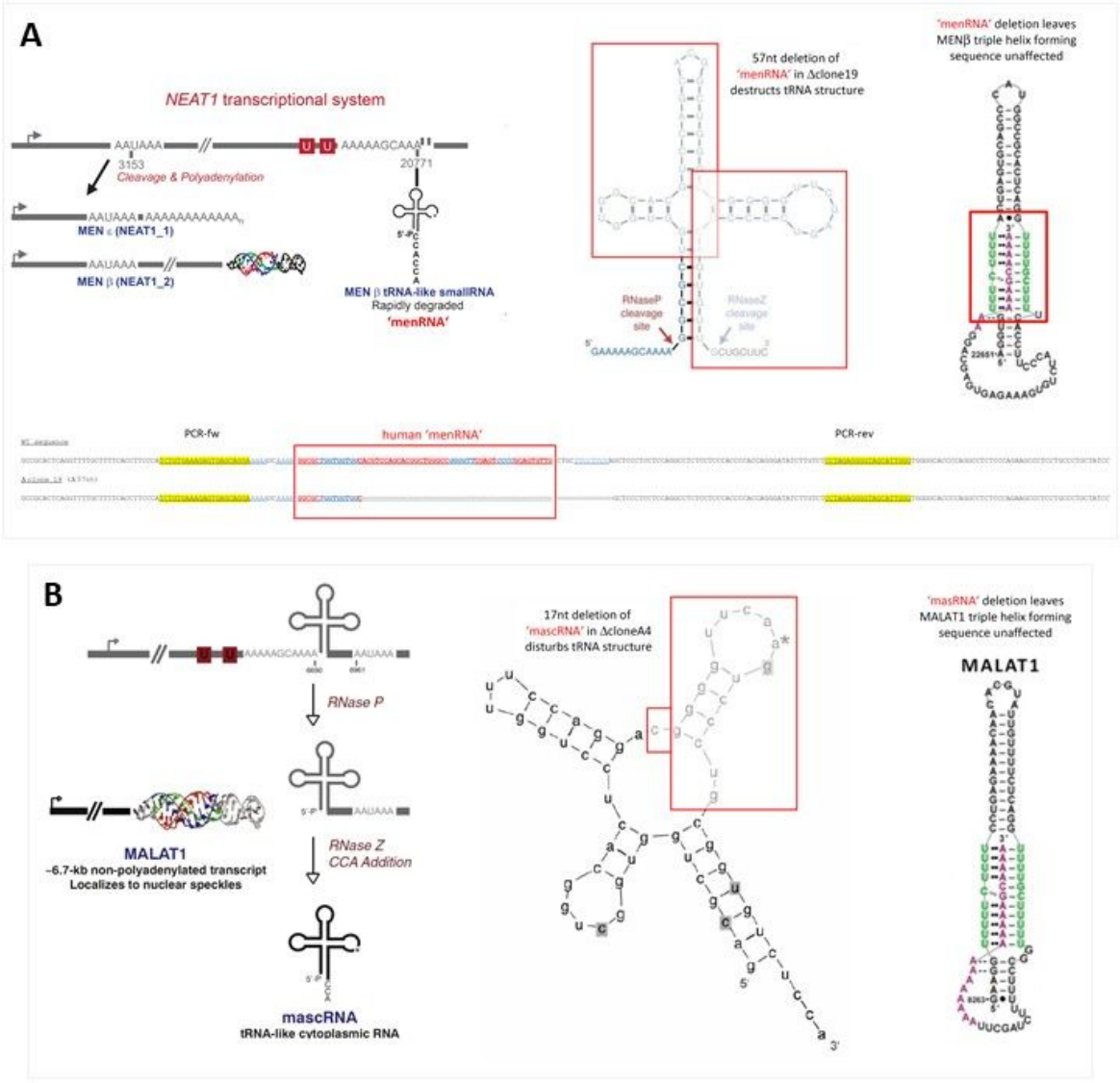

Figure 1

Panel A: The *NEAT1-MALAT1* gene cluster encodes two primary transcripts which are subsequently processed to transcripts of vastly different size. The *NEAT1* locus yields the 23kb MENβ (NEAT1_1) and 3.7kb MENε (NEAT1_2). Of note, the long MENβ transcript forms an unusual triple helix structure at its 3'-end which has been shown to stabilize this long transcript. From the primary transcript, an additional short tRNA-like 59nt 'menRNA' is generated through RNAse P and Z enzymatic cleavage.

Panel B: The MALAT1 locus yields a 8.3 kb primary transcript also forms a stabilizing triple helix at the 3'-end, and through enzymatic cleavage another small tRNA-like 59nt 'mascRNA'. Using CRISPR-Cas9, we developed human monocyte-macrophage cell lines with menRNA or mascRNA sequence deletions as indicated. These editing procedures do not affect the lncRNA parent transcript or triple-helix structure formation.

Figure 1

Targeted deletion of tRNA-like transcripts from the NEAT1-MALAT1 cluster Panel A: The NEAT1-MALAT1 gene cluster encodes two primary transcripts which are subsequently processed to transcripts of vastly different size. The NEAT1 locus yields the 23kb MENβ (NEAT1_1) and 3.7kb MENε (NEAT1_2). Of note,

the long MENβ transcript forms an unusual triple helix structure at its 3'-end which has been shown to stabilize this long transcript. From the primary transcript, an additional short tRNA-like 59nt 'menRNA' is generated through RNAse P and Z enzymatic cleavage. Panel B: The MALAT1 locus yields a 8.3 kb primary transcript also forms a stabilizing triple helix at the 3'-end, and through enzymatic cleavage another small tRNA-like 59nt 'mascRNA'. Using CRISPR-Cas9, we developed human monocyte-macrophage cell lines with menRNA or mascRNA sequence deletions as indicated. The editing procedures occur outside of the primary transcript sequences required for regular formation of the triple-helix structures at their 3'-ends which support stabilization of the respective lncRNAs. Under the experimental conditions employed there was no change in NEAT1 expression as detectable by RNA-sequencing (RNA-seq) and qRT-PCR. For a high resolution version of this figure please refer to the Supplement. Further details regarding the targeted genomic regions (Suppl. Fig. S1AB), recombinant expression and Northern blot analysis of menRNA (Suppl. Fig. S1CD), structure prediction for residual transcripts (Suppl. Fig. S2), in vitro transcription of single-guide RNAs for CRISPR-Cas9 experiments (Suppl. Fig. S3A), and PCR analysis and sequencing of the deletion clones (Suppl. Fig. S3BC) are provided in the Supplement.

Figure 2 Gene set enrichment analyses of ΔmenRNA monocytes (*Panel A*) and ΔmascRNA monocytes (*Panel B*)

Figure 2

Gene set enrichment analysis of ΔmenRNA and ΔmascRNA monocytes RNA-seq identified profound alterations in the baseline transcriptomes of ΔmenRNA (panel A) and ΔmascRNA (panel B) monocytes. Depicted is a gene set enrichment analysis (GSEA) of the RNA-seq datasets, mapped against gene sets from the Molecular Signature Database's (MSigDB) collection derived from the Kyoto Encyclopedia of

Genes and Genomes (KEGG) pathway database. For a high resolution version of this figure please refer to the Supplement. Further details regarding the RNA-seq analyses are provided in Suppl. Tables S1/S2.

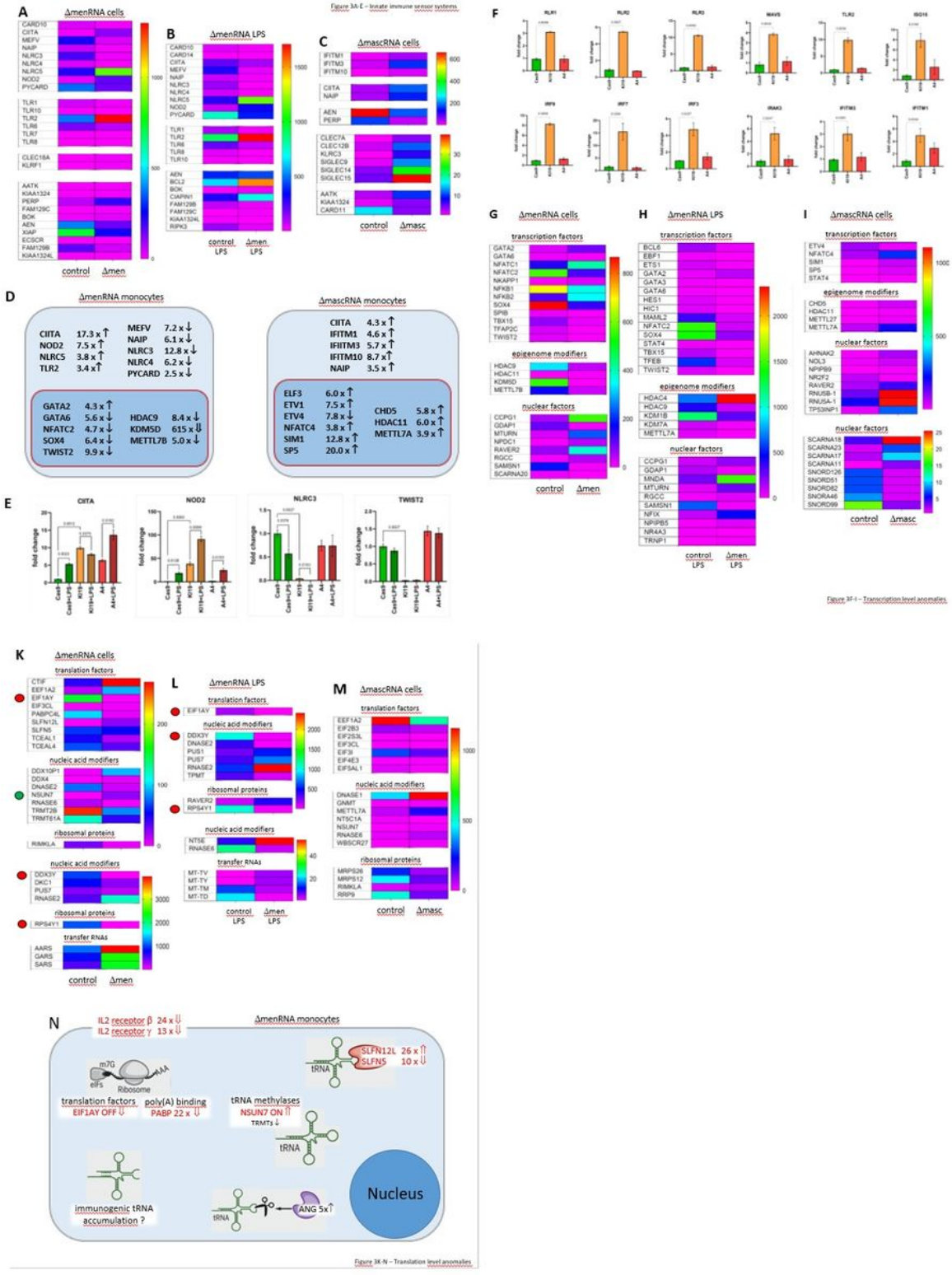

Figure 3

Disturbances of innate immune sensing, transcription and translation in defective monocytes Panels A-E (Innate immune sensing) A key finding of the RNA-seq was imbalance between multiple innate immune

sensors in ΔmenRNA cells under baseline (panel A) and LPS-stimulated (panel B) conditions (Table S1A). Amongst cytosolic receptors, NOD2 10 was 8- fold and CIITA 65 17-fold induced, whereas NLR-class receptors NLRC3, NLRC4, NAIP and MEFV 12 were suppressed in ΔmenRNA monocytes. Amongst membrane-bound Toll-like receptors, TLR 2 showed 10-fold elevated baseline expression in ΔmenRNA cells. In contrast, defective induction was seen for TLR6, TLR1, TLR8, TLR10, and TLR7 in ΔmenRNA upon LPS challenge (panel B). In the context of the observed massive baseline induction of NOD2 and TLR2 it is notable that twist family bHLH transcription factor 2 (TWIST2) 15 was 10-fold down in these ΔmenRNA cells (panels GH), and that loss of NLRC3 and TWIST2 expression in ΔmenRNA monocytes could not be rescued by LPS (panel E, compare Fig. 6A for related findings in macrophages). mascRNA cells likewise displayed anomalies in immune sensor expression (panel C)(Table S2A), however different from those observed in ΔmenRNA cells. Prominent in ΔmascRNA monocytes was the induction of interferon (IFN)-induced transmembrane (IFITM) proteins which represent primary cellular defenses against multiple viruses 16. Upon PMA-induced differentiation of ΔmenRNA and ΔmascRNA monocytes into macrophages multiple further baseline anomalies of antiviral defense genes became apparent (Suppl. Fig. S9). In both defective clones there was imbalance of apoptosis-related genes. In LPS-stimulated ΔmenRNA cells (panel B) apoptosis regulator BOK and Niban apoptosis regulator FAM129C were upregulated, whereas serine/threonine kinase RIPK3 and apoptosis inhibitor NAIP and CARD14 were suppressed here. In ΔmascRNA cells (panel C), NAIP was induced while apoptosis enhancing nuclease AEN 66 was 3.-fold and p53 apoptosis effector PERP 67 5.1-fold suppressed (Table S2A). Page 22 of 26 In addition to alterations of protein-coding genes, RNA-seq identified deregulation of long noncoding RNAs (lncRNAs) and antisense (AS) RNAs in ΔmenRNA and ΔmascRNA monocytes (Tables S1D/2D). Thus, ΔmenRNA cells showed 7- fold downregulation of a recently discovered novel transcript designated 'MARCKS cis-regulating lncRNA promoter of cytokines and inflammation' or 'regulator of cytokines and inflammation' (ROCKI) (see Fig. 4DE)(Tables S1D/S2D). This transcript of particular interest was identified by Zhang et al. 23 conducting a genome-wide scan of TLR-stimulated macrophages for pairs of cis-acting lncRNAs and protein-coding genes involved in innate immunity. Panels F-I (Transcriptional level) Several transcription factors (TF), nuclear factors and epigenome modifiers were deregulated in defective cells. At the transcriptional level, in addition to TWIST2, TF GATA2 was 4-fold induced and GATA6 20-fold suppressed, and NFATC2 switched off in ΔmenRNA cells (panels GH) at baseline already (compare Fig. 5AD for related findings in macrophages). Further TFs (SOX4, ETS1, STAST4) and epigenome modifiers turned into disequilibrium upon LPS challenge, among them histone deacetylases (HDAC4, HDAC9, HDAC11), lysine demethylases (KDM1B, KDM7A), and METTL methyltransferase family members 17 known or predicted to methylate DNA, RNA or proteins (METTL7A, METTL7B). Panel D summarizes the most prominent changes of cytosolic and membrane-bound innate immune sensors, and of transcription factors and epigenome modifiers, in ΔmenRNA and ΔmascRNA monocytes. Panel E exemplifies how LPS-stimulation exacerbates several of these deregulations (e.g. CIITA and NOD2) while this stimulation it is uncapable to overcome certain blocks (e.g. of NLRC3 or TWIST2)(see Fig. 6A for related findings in macrophages). Bar graphs show means ± SE from three biological replicates. Panels K-N (Translational level) Particular anomalies were identified regarding translation factors, ribosomal proteins and nucleic acid modifiers in ΔmenRNA (panels KL) as well as

ΔmascRNA monocytes (panel M). In ΔmenRNA cells the translation initiation and elongation factors EIF3CL, EEF1A2, and CTIF were induced, whereas the initiation factor EIF1AY was completely silenced 18. DEAD-box helicase DDX3Y and ribosomal protein RPS4Y1 were switched off, too, in menRNA-deficient cells under baseline conditions (panel K) and these shutdowns persisted upon LPS stimulation of the cells (panels L). By contrast, RNA methyltransferase NSUN7 which is able to reinforce transcription concomitant with m(5)C marks on enhancer RNAs 19,21, was switched on in ΔmenRNA monocytes (panel K) while undetectable in control cells. At the level of tRNAs, genomically or mitochondrially encoded tRNAs 20,21 and tRNA methyltransferases (TRMT61A, TRMT2B) displayed major deregulation in ΔmenRNA cells (panel KL). ΔmascRNA cells (panel M), on the other hand, showed none of these alterations, whereas cytosolic nucleotidase NT5C1A 22 which dephosphorylates the 5' and 2'(3')-phosphates of deoxyribonucleotides and has broad substrate specificity, is ≈10-fold suppressed here. Panel N summarizes major changes regarding the translational machinery in menRNA-deficient monocytes, including translation factors and a poly(A) binding protein, tRNA methylases, two SLFN family members, angiogenin (ANG), and IL2 receptor subunits β and γ. These alterations within the translation system of ΔmenRNA monocytes may lead to accumulation of anomalous tRNAs and tRNA fragments (tiRNAs, tsRNAs), in particular under conditions of cellular or immune stress (for details see the discussion section Loss of nucleus-to-cytosol supply of menRNA or mascRNA).

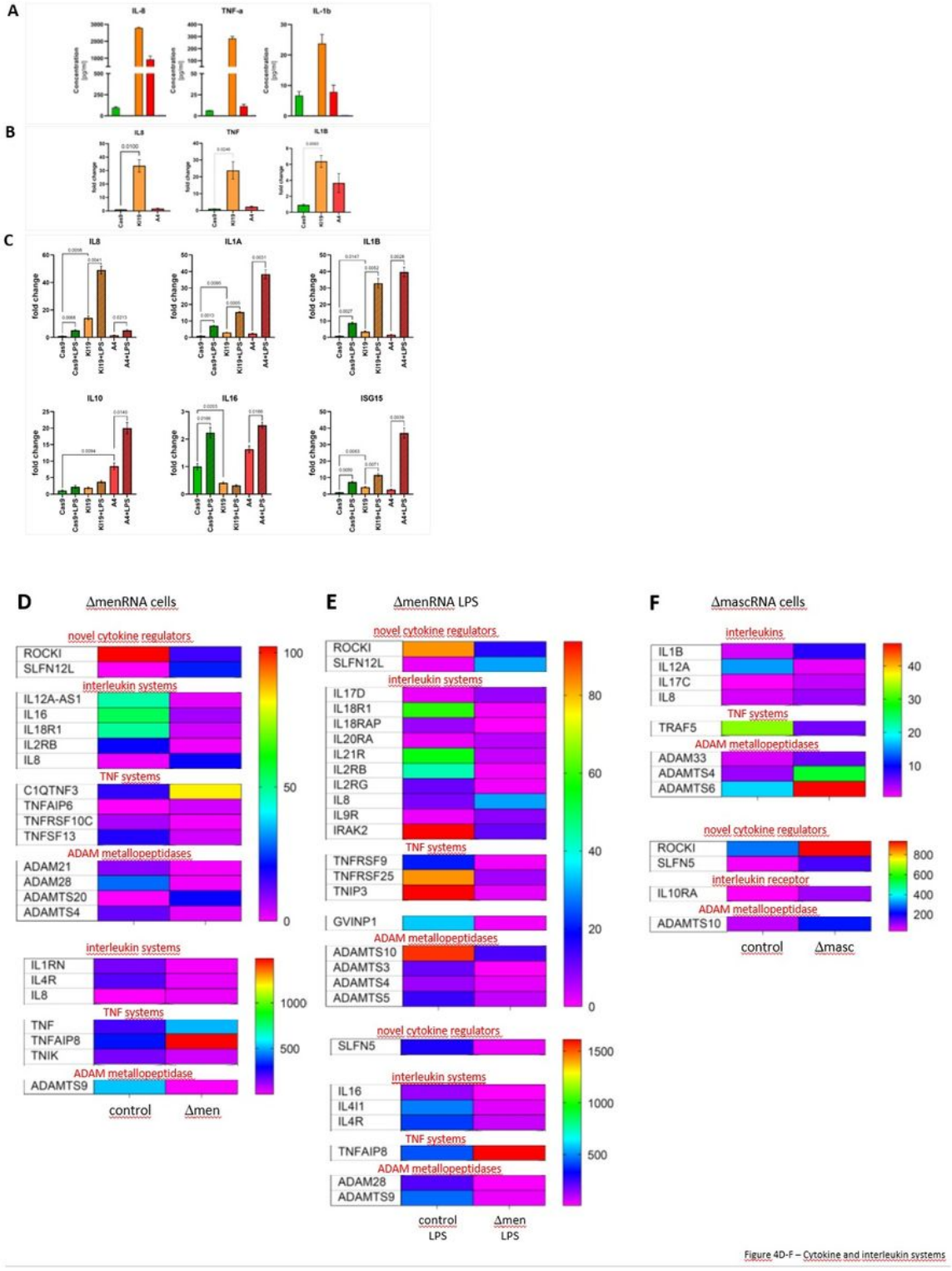

Figure 4D-F – Cytokine and interleukin systems

Figure 4

menRNA and mascRNA deletion results in loss of cytokine control and imbalance of interleukin systems Panel A: Prominent was massively elevated expression and secretion of the IL-8, TNF, and IL1B in unstimulated ΔmenRNA cells. Cytometric bead assay protein data on media conditioned by control monocytes (green), ΔmenRNA (orange), and ΔmascRNA cells (red). Panel B: qRT-PCR quantification of gene expression levels. For all three proinflammatory cytokines, ΔmenRNA displayed far more

pronounced induction than ΔmascRNA cells. Panel C: ΔmascRNA monocytes displayed exaggerated induction of IL1A, IL1B, IL10, and ISG15 expression upon LPSstimulation as compared to controls. Only stimulated ΔmenRNA cells showed a further increase of IL8 expression, whereas IL16 68 was suppressed in this clone at baseline, and failed to become induced upon LPS challenge. Panels D-F: RNA-seq identified further anomalies of IL and TNF systems. Among receptors, IL4R was ▯7-fold and IL4- induced gene (IL4I1) ▯11-fold suppressed in stimulated ΔmenRNA cells (panels DE). Even more pronounced was disequilibrium in the IL18 system (IL18R1 >70-fold inhibited, IL18 receptor accessory protein IL18RAP switched off). In the IL2 system, receptor subunit IL2R-β was ▯52-fold and IL2R-γ ▯13-fold suppressed in LPS-stimulated ΔmenRNA monocytes (panel E). Regarding the IL1 system, IL1 receptor antagonist IL1RN was ▯12-fold and IL1 receptor associated kinase IRAK2 ▯8-fold down in ΔmenRNA cells. Among the ligands, IL16 expression remained ▯18-fold blunted even upon LPS-challenge (compare panel C).

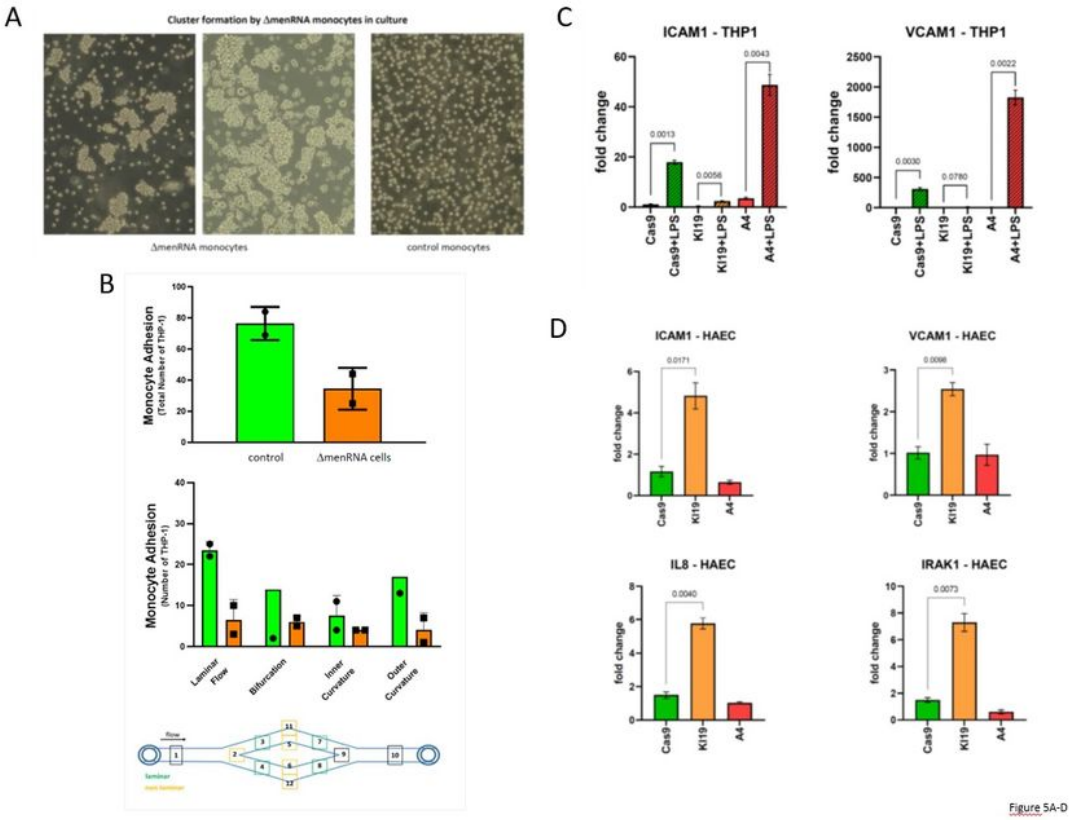

Figure 5A-D

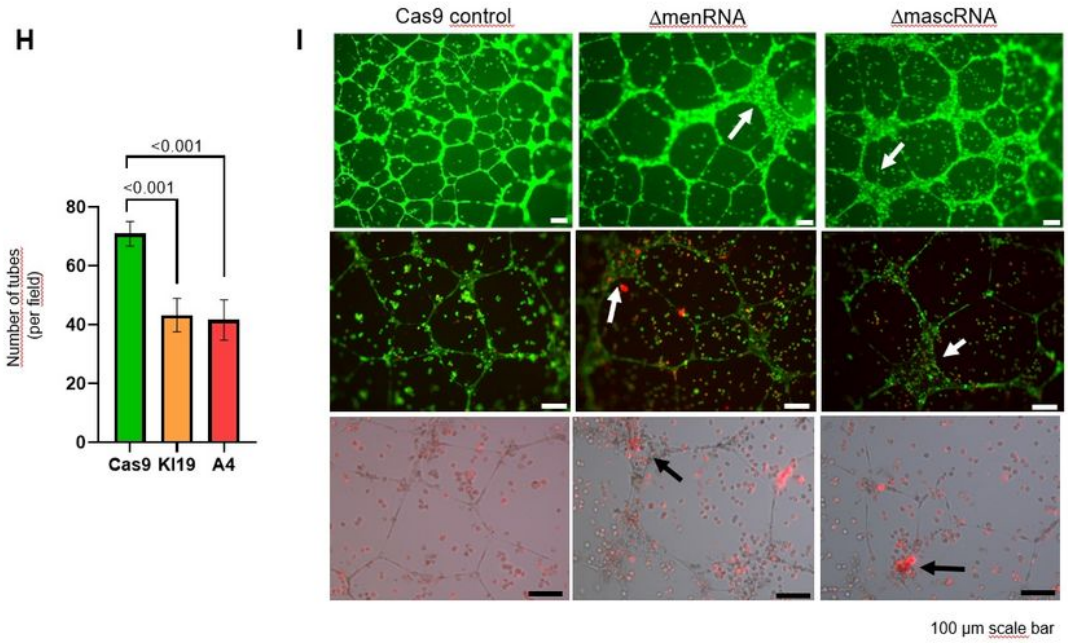

Figure 5

Impact of menRNA and mascRNA deletions upon monocyte-endothelium interactions and angiogenesis For a high resolution version of this figure please refer to the Supplement. Panels A-D (Endothelial cell interactions) At the cellular level, ΔmenRNA monocytes displayed an anomalous growth pattern with spontaneous cell cluster formation in liquid culture (panel A). Despite this morphological anomaly, there was no significant difference in their cell proliferation kinetics compared to ΔmascRNA and control

monocytes (data not shown). ΔmenRNA cell showed defective endothelial adhesion under multiple flow conditions (panel B). While expression of vascular cell adhesion molecule 1 (VCAM-1) was ▯200-fold induced by LPS, starting from a very low baseline level in control cells, this induction was almost entirely blunted in ΔmenRNA cells. Similarly, the LPS-dependent induction of ICAM1 was strongly reduced in these defective cells (panel C). Transfer of ΔmenRNA monocyte-conditioned medium to HAEC endothelial monolayers triggered changes in the expression of multiple genes including ▯10-fold increased ISG15, ▯8-fold increased IL8, ▯7-fold increased IRAK1, ▯7-fold increased ICAM1, whereas ΔmascRNA-conditioned medium exerted no such influence. Bars graphs show means ± SE from two biological replicates (panel D). Panels E-G (Cell adhesion molecule profiles) RNA-seq identified profound deregulation of multiple cell adhesion molecules in ΔmenRNA cells (panels EF) including adhesion G protein-coupled receptors (GPRs, BAIs) 40, intercellular adhesion molecules (ICAMs), neural cell adhesion molecules (NCAMs), integrins (αM, αL, αX, α1, α4, α6, β7), vascular cell adhesion molecule (VCAM1), and ESAM (endothelial cell-specific adhesion molecule). ΔmascRNA cells (panel G) displayed deregulation of several cell adhesion molecules, too, however distinct from those observed in ΔmenRNA cells. Thus, neuronal growth regulator NEGR1, involved in neuronal growth and connectivity and cell-cell interactions in general, is ▯28-fold down in Δmen19 while unaltered in Δmasc19 cells. Cytoskeleton regulating NCKAP1 was ▯14-fold increased in ΔmascRNA while unaltered in ΔmenRNA cells. Panels H-M (Angiogenesis, growth factors and chemokine systems) Quantitative effects of both ΔmenRNA (orange) and ΔmascRNA (red) monocyte-conditioned media upon HAEC-based tube formation in an angiogenesis assay, as compared to Cas9 controls (green). Supernatant from each of the defective cell clones highly significantly reduced the number of tubes formed. Bars graphs show means ± SE from three biological replicates (panel H). Beyond a quantitative effect of secreted factors from the cells, direct co-culture of ΔmenRNA as well as of ΔmascRNA monocytes with the HAECs lead to profound alterations of HAEC cell morphology. In co-cultures with any of the defective monocytic clones, there was a massive increase in the size of HAECs at many branch side nodes where ≥3 endothelial cells came into contact (white arrows in the upper and middle rows). When the defective monocytes clones were red-stained (with DiI) before addition to the HAEC-matrigel mixture, there was significant accumulation of red cells (black arrows in the lower row) at branch side nodes where HAEC hypertrophy occurred (panel I). Multiple growth and angiogenesis-associated factors as well as chemokines were in disequilibrium in both ΔmenRNA (panels KL, table S1G) and ΔmascRNA monocytes (panel M, table S2G). Compared to controls, ΔmascRNA monocytes showed ▯12-fold increased baseline expression of angiogenin (ANG), a key protein of angiogenesis interacting with endothelial and smooth muscle cells resulting in cell migration, invasion, proliferation and formation of tubular structures. Beyond these properties, ANG exhibits ribonucleolytic activity critical for its biological functions and is also involved in nucleic acid metabolism. ΔmascRNA cells (panel M) displayed induction of angiopoietins ANGPT1 and ANGPT4, angiopoietin-like 4 (ANGPTL4), and vascular endothelial growth factor (VEGFA). While ΔmenRNA monocytes likewise showed induction of VEGFA, angiopoietin like 6 (ANGPTL6) was ▯7-fold down and ANGPT1 shut off here. Within the transforming growth factor system, TGF β2 (TGFB2) expression was undetectable in controls but strongly induced in ΔmenRNA cells (panels KL). Similarly, one latent TGF β-binding protein (LTBP1) and TGFBR3L were induced from low baseline levels. Conversely, TGF β3 (TGFB3) was downregulated as well as the TGF β-induced gene TGFBI. GREB1,

a suppressor of TGF-β signaling, was undetectable in controls, but high in ΔmenRNA cells. ΔmascRNA monocytes (panel M) also displayed significant TGF system deregulation, but distinct from ΔmenRNA cells. Thus, TGF α (TGFA) was 8-fold induced in ΔmascRNA cells while TGF β2 expression was unchanged. Another latent TGF βbinding protein (LTBP2) and TGF β induced (TGFBI) gene were upregulated here. Insulin like growth factor (IGF) system is likewise disturbed, and growth differentiation factors including GDF5, a bone morphogenetic protein (BMP) ligand from the TGF-β superfamily. While two chemokine receptors (CXCR4 and CCR2) were 3-fold induced in stimulated ΔmenRNA cells (panels KL), CX3-C chemokine receptor 1 (CX3CR1) (fractalkine receptor) displays 9-fold reduced expression. Receptors CCR7 and Page 24 of 26 CXCR3 were massively 44-fold suppressed in ΔmenRNA cells. Among ligands, CXC-type CXCL10, CXCL11, CXCL13, and CXCl16 displayed up to 10-fold suppressed expression in this clone.

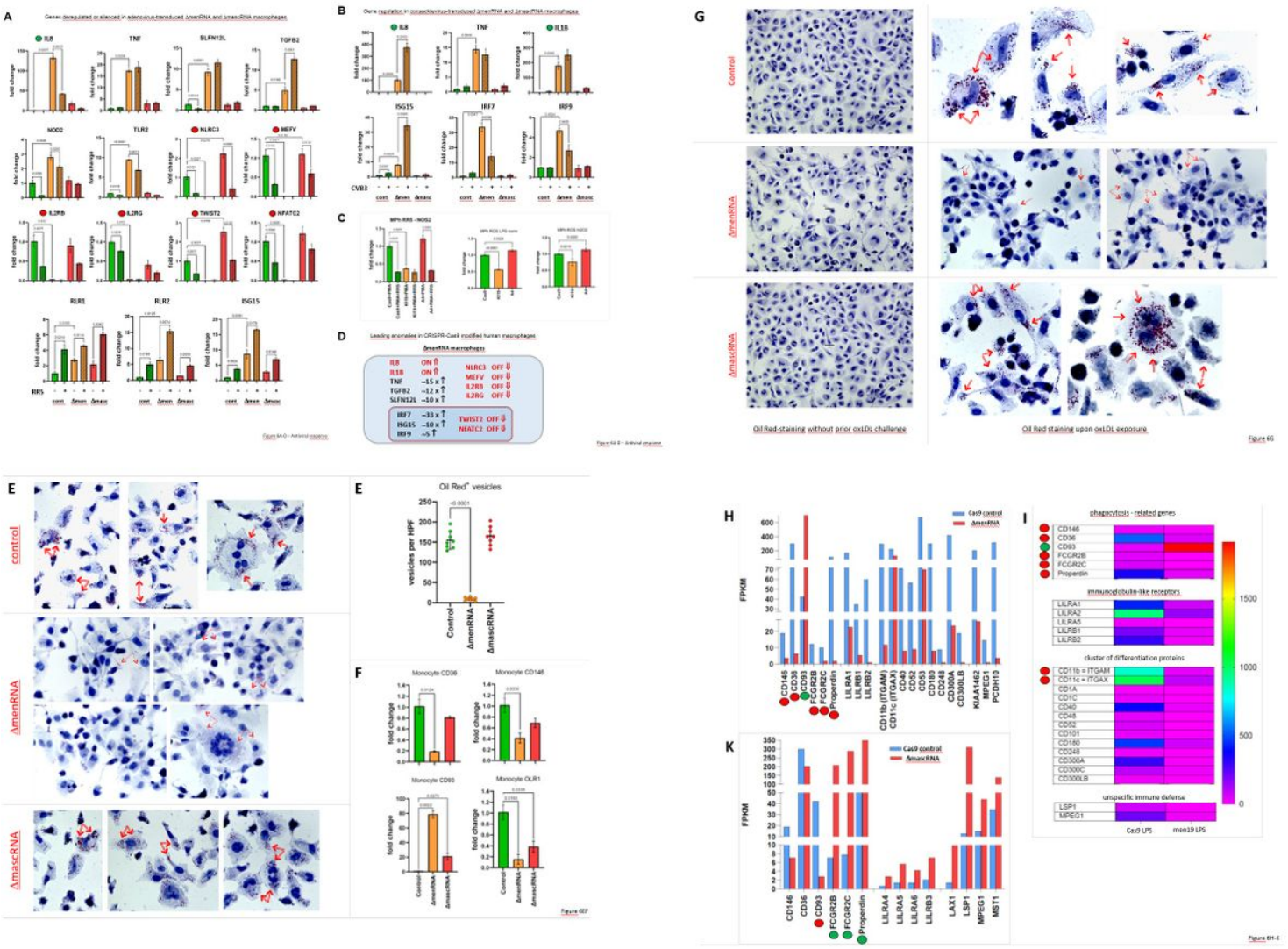

Figure 6

Antiviral response, foam cell formation and oxLDL uptake of ΔmenRNA and ΔmascRNA macrophages For a high resolution version of this figure please refer to the Supplement. Panels A-D (Response to human-

pathogenic viruses) PMA-induced differentiation of ΔmenRNA cells to adherent macrophages rendered the cells susceptible to efficient transduction by recombinant viruses derived from the human-pathogenic double-stranded DNA (dsDNA) adenovirus type 5. At a multiplicity of infection (MOI) 25, the GFP-expressing virus AdV-CMV-GFP efficiently transduced these macrophages, resulting in strong GFP expression in >50 % of cells (Suppl. Fig. S8A). In thus generated macrophages, without LPS stimulation or virus exposure, the IL8 expression level was massively ≈130-fold compared to controls (panel A). Transduction with a recombinant adenovirus without the GFP expression cassette (AdV-RR5) resulted in a significant decrease of IL8 expression level in these ΔmenRNA cells, to ≈40-fold of the level in control macrophages. In contrast, control cells displayed no change of their very low baseline IL8 expression, in response to AdV-RR5. ΔmenRNA macrophages showed ≈17-fold higher baseline TNF expression compared to controls. Transduction with AdV-RR5 resulted in no significant change of TNF transcription, neither in ΔmenRNA nor control cells. Similarly, TLR2 expression was ≈5-fold higher in ΔmenRNA macrophages vs. controls, without changes in response to AdV-RR5. Several other genes were induced in response to transduction (RIG-like receptors RLR1 and RLR2, ISG 15), but without significant differences between defective and control cells. Striking was a complete shutdown of several genes already suppressed in ΔmenRNA monocytes (Fig. 3A-E, Fig. 4EF) before their transformation into macrophages: NOD-like innate immune genes NLRC3 and MEFV, IL2 receptor subunits β and γ, transcription factor TWIST2, and NFATC2. None of these genes fully silenced in macrophages could be 'rescued' by adenovirus exposure, similar to findings in LPSstimulated monocytes (Fig. 3A-E, Fig. 4EF). Bar graphs show means ± SE from three biological replicates. Panel B shows the response of ΔmenRNA macrophages to Coxsackievirus B3, an important human-pathogenic singlestranded RNA (ssRNA) virus. Their IL8 response to CVB3 (≈5-fold induction upon virus exposure) was opposite to that to AdV-RR5 (reduction of IL8 to ≈2/3 of the high baseline level). Efficient transduction by CVB3 was detected by qRTPCR, while CVB3 (-) minus strand-specific RT-PCR indicative of active replication was negative for all clones (Suppl. Fig. S8B). Bar graphs show means ± SE from two biological replicates. Panel C displays blunted NOS2 expression (qRTPCR) by ΔmenRNA but not ΔmascRNA macrophages at baseline and upon adenovirus exposure, as well as impaired ROS production after LPS or H2O2 challenge. Bars graphs show means ± SE from three biological replicates. Panel D summarizes the leading anomalies in CRISPR-Cas9 modified human ΔmenRNA macrophages. Panels E-K (Foam cell formation and oxLDL uptake) Panels E-G: Whereas ΔmascRNA macrophages displayed an oxLDL uptake pattern undistinguishable from that of control cells (intracellular Oil Red-positive OR+ vesicles as indicated by red arrows). In contrast, essentially no normalsized intracellular OR+ vesicles were observed in ΔmenRNA macrophages ($p < 0.0001$) 24 hrs after oxLDL exposure. A minor number of very small OR+ particles is visible in ΔmenRNA cells. It appears these minute particles are not artifacts, and do not represent spontaneous intracellular accumulation of any OR+ material in the ΔmenRNA cells, but residues of defective oxLDL endocytosis since they do not show up without prior oxLDL challenge (panel G). For high resolution microphotographs please refer to the figure's source file. The striking defect of oxLDL uptake by ΔmenRNA macrophages is paralleled by loss of scavenger receptors CD36, MCAM (CD146)69, MSR1, and OLR1 (LOX1) 70 (panel F). Bars graphs show means ± SE from four biological replicates. Panels H-K: These changes occur in the context of further anomalies, identified by RNA-seq of monocytes, affecting

phagocytosis as an evolutionarily conserved general defense mechanism involving, beyond scavenger receptors, Fcγ receptors (FcγRs) 44,45 and complement receptors (CRs). FCGR2 genes encoding Fc fragments of inhibitory FcγRIIB are suppressed in ΔmenRNA cells and not rescuable by LPS (panel HI). Complement component properdin (CFP) is likewise down. Of note, ΔmascRNA cells (panel K) display opposed deregulation of the same FCGR2 genes, and induction of properdin and other complement components. Remarkable is also strong opposed deregulation of CD93 in ΔmenRNA compared to ΔmascRNA monocytes. While massively induced in ΔmenRNA cells, CD93 was shut down in ΔmascRNA monocytes, contrasting with robust expression in controls. CD93 is a lectin receptor involved in control of the immune response 37. Another distinction between the defective clones regards MPEG-1 (perforin-2), an evolutionary ancient protein involved in the unspecific immune defense 38, which was ⍰16-fold down in ΔmenRNA while upregulated in ΔmascRNA cells. Page 25 of 26 Scavenger receptor CD36 30,32 was ⍰48-fold down in ΔmenRNA monocytes. They also show suppression of Cluster of Differentiation (CD) marker CD40, a member of the TNF receptor family, and of CD52, a glycoprotein modulating Tcell activation. CD300A and CD300C, involved in viral immune evasion, were ⍰26-fold and ⍰5-fold suppressed, respectively. None of the group 1 CD1 molecules, normally expressed on cells specialized in antigen presentation, could be induced by LPS-treatment of ΔmenRNA cells. Finally, leukocyte immunoglobulin like receptors (LILRs) were broadly deregulated. ΔmascRNA cells (panel K) displayed none of these ΔmenRNA-associated CD molecule or LILR deregulations.

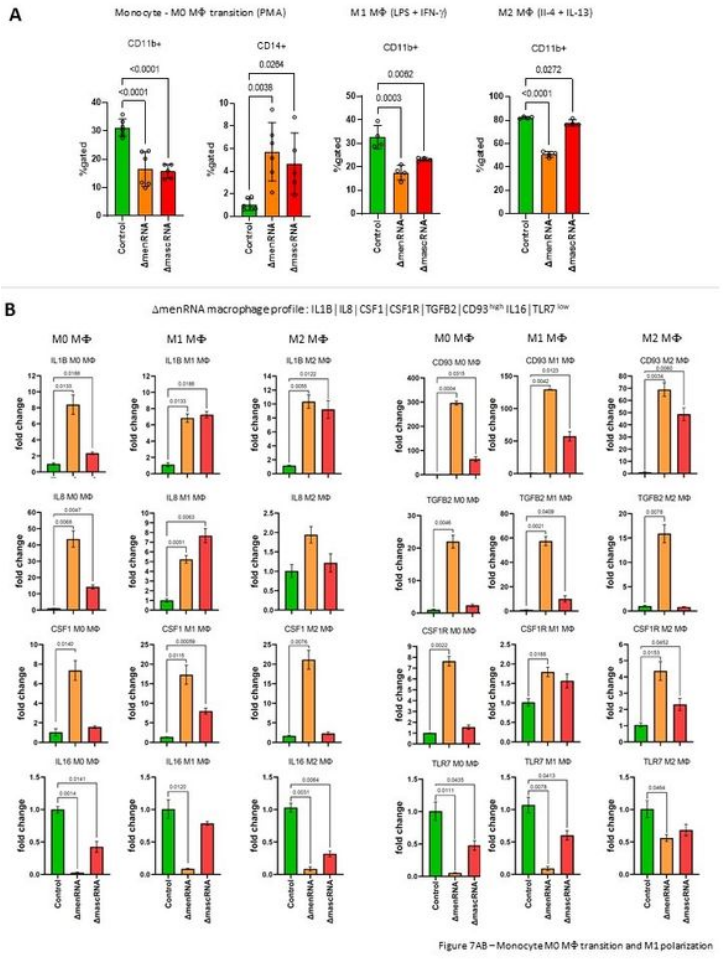

Figure 7AB – Monocyte M0 MΦ transition and M1 polarization

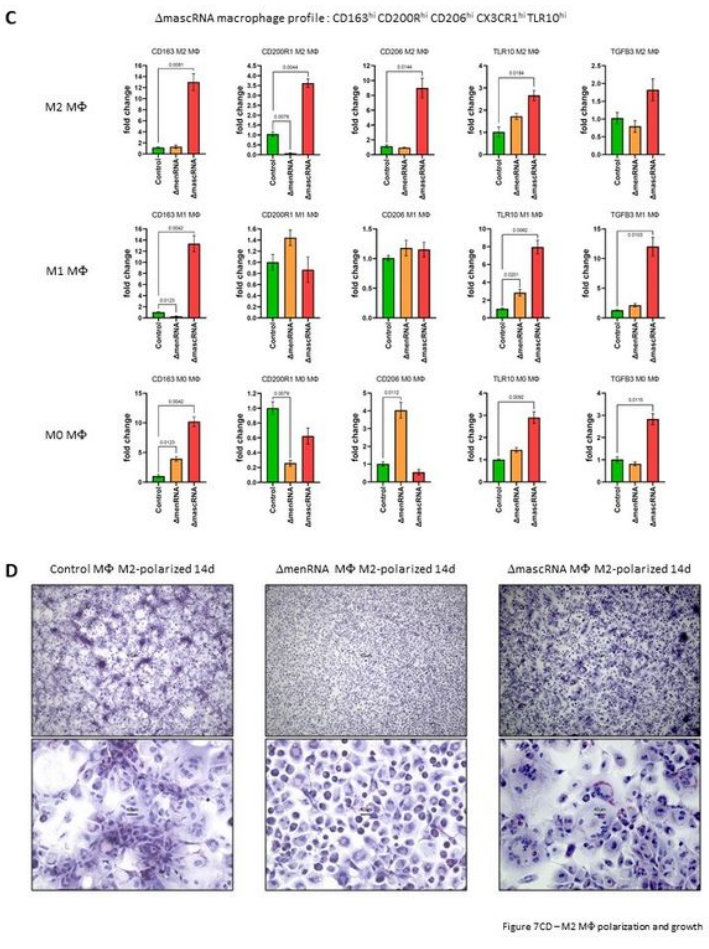

Figure 7CD – M2 MΦ polarization and growth

Figure 7

Anomalous monocyte-macrophage differentiation and polarization For a high resolution version of this figure please refer to the Supplement. Whereas the monocyte clones had similar proliferation kinetics in liquid culture (Fig. 5A), they differed with respect to their macrophage differentiation and response to polarization agents. Monocyte-M0 macrophage differentiation and subsequent M1/M2 macrophage polarization were conducted as follows: First, M0 macrophages were generated by incubation of THP-1 monocyte clones for seven days, with PMA at a concentration of 100 ng/ml. Thereafter, the cells were further incubated for another seven days, either with IFN-γ at 20 ng/ml plus LPS at 100 ng/ml to induce M1 polarization, or with IL-4 at 20 ng/ml plus IL-13 at 20 ng/ml to induce M2 polarization. 'M0' expression profiles and FACS data in panels A-C were obtained on day 7 of culture. The 'M1' and 'M2' expression profiles in panels BC were obtained on day 14 of culture. Expression profiling allowed unequivocal distinction between each of the three clones (ΔmenRNA, ΔmascRNA, controls). Panel A: ΔmenRNA monocytes were uncapable of normal differentiation into M0 macrophages upon PMA exposure, consistent with the grave disturbance of CD molecule expression in these monocytes (including CD11b, CD11c). In accordance with these transcription level alterations, FACS analysis identified defective transition from monocytes (both ΔmenRNA and ΔmascRNA) to M0 macrophages as assessed by CD11b and CD14 expression. The graphs display the statistics of 5-6 independent biological samples (one-way ANOVA multiple comparisons, FACS gatings in Suppl. Fig. S9B). Panel B: A distinctive expression profile was characteristic of ΔmenRNA cells. It was previously observed in ΔmenRNA monocytes (Fig. 4A-C), ΔmenRNA M0 macrophages, and preserved upon their treatment with M1 or M2 polarization protocol. This conserved pattern encompasses IL1B, CD93, TGFB2, CSF1 and its receptor CSF1R. While high proinflammatory IL1B expression is common to M1-polarized cells, the massive induction of CD93 or the CSF1 - CSF1 receptor system 51 observed here is not commonly associated with either M1 or M2 polarized cells. Bars graphs in panels B and C show means ± SE from four biological replicates. The expression levels of each gene are normalized to the control clone level at the respective time, i.e. day 7 for M0 macrophages, and day 14 for M1 and M2 polarized cells. Panel C: Beyond M0 differentiation, another characteristic expression profile developed for ΔmascRNA cells. A "M2- prone" pattern comprising CD163hi CD200R1hi CD206hi CX3CR1hi TLR10hi was observed in ΔmascRNA macrophages upon the M2 polarization protocol. This is easily distinguished from the profile of control and ΔmenRNA cells after this treatment. TLR10 was recently identified as anti-inflammatory pattern-recognition receptor 49 and added to this "M2-prone" pattern. Panel D: At the end of the 14 days M2 polarization protocol, the morphological aspect of M2-polarized ΔmenRNA macrophages was grossly different from that of control cells and ΔmascRNA cells. At that time, "colony-like" cell clusters became visible in both control and ΔmascRNA cultures, whereas the distribution of the M2-polarized ΔmenRNA macrophage remained essentially homogeneous. For high resolution microphotographs please refer to the Supplement.

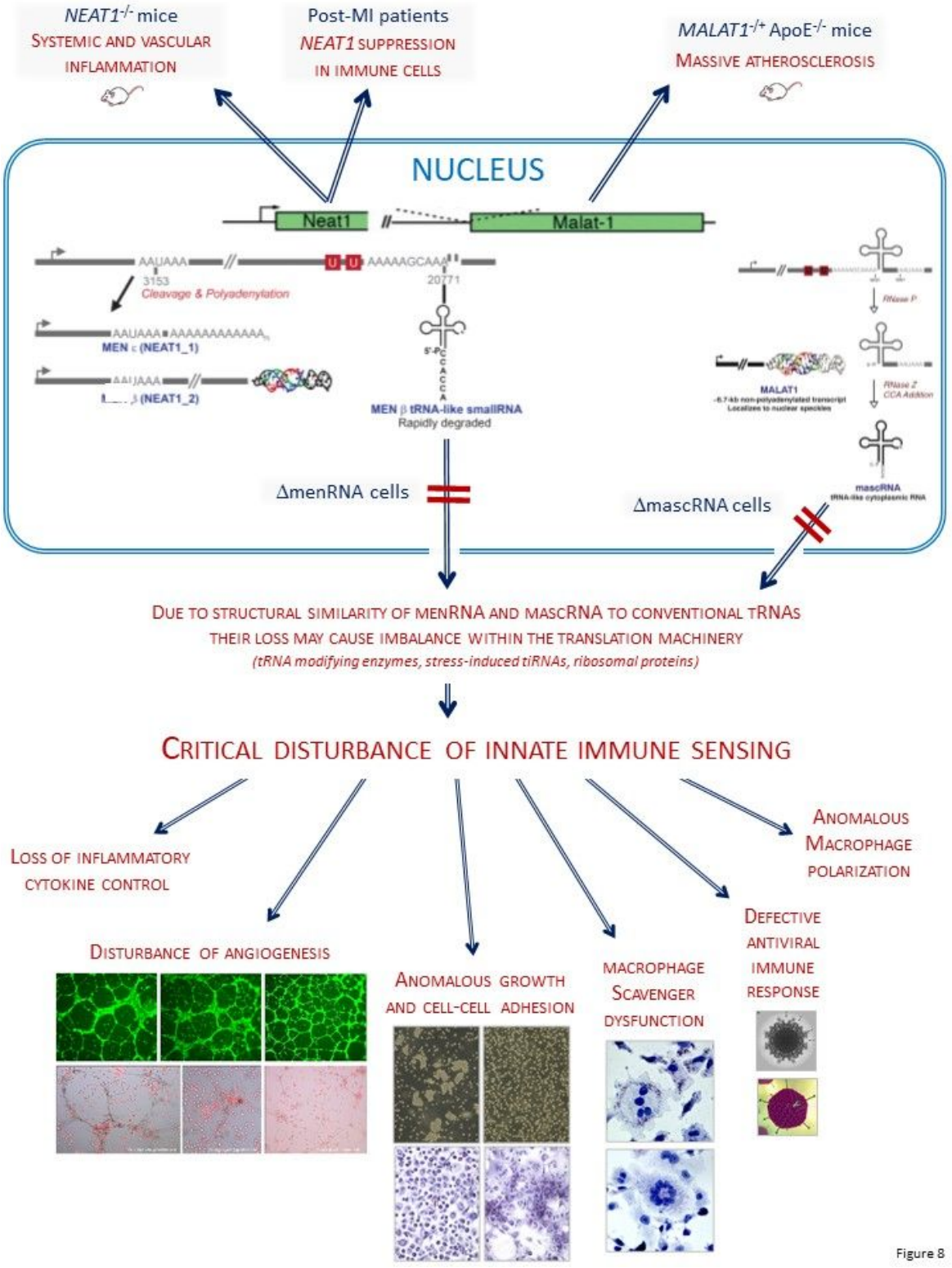

Figure 8

Summary figure and working model Analysis of monocytes-macrophages carrying narrowly targeted deletions of the novel tRNA-like molecules indicates they are critical building blocks required for balanced function of innate immunity. The grave disturbance of multiple immune sensor systems - with complex downstream sequelae – might be addressed by a working hypothesis invoking a primordial defect linked to the peculiar structure of menRNA and mascRNA. They closely resemble common tRNAs, strongly

suggesting that they also interact with the ribosomal machinery. Accordingly, ablation of nucleus-to-cytosol supply of menRNA or mascRNA would cause imbalance within the translation system, consistent with the observed Page 26 of 26 deregulation of multiple translation factors, tRNAs, tiRNAs, and ribosomal proteins in defective cells. Delineation of a specific molecular mechanism to prove this hypothesis is far beyond the scope of this study which attempted to first identify any distinct biological functions of menRNA and mascRNA within the NEAT1-MALAT1 cluster. Considering the minute and narrowly targeted genetic interventions employed, the extent of disturbances from key innate immune sensors to complex downstream sequelae, is unexpected. Beyond primary defects at sensor level, the grave loss of cytokine control, angiogenesis-modifying effects of ΔmenRNA and ΔmascRNA monocytes, and defects of key ΔmenRNA and ΔmascRNA macrophage functions, constitute the first known biological functionalities of these cytosolic molecules. From this starting point it appears warranted to generate murine models, with cell type-specific inducible knockout of menRNA or mascRNA only, to further elucidate their functions in disease models. For future translational studies, our approach to study menRNA and mascRNA directly suggests new avenue since their highly dynamic levels may be more closely related to clinical parameters and clinical course than those of their nuclear precursors. They may also have value as therapeutic targets for pharmacological intervention since they are more easily accessible than their extremely complex nuclear-located precursor molecules. A prior observation that recombinant mascRNA 3 abolishes virus replication in cardiomyocytes does suggest potential of mascRNA- and menRNA-targeting interventions. From an evolutionary perspective, the NEAT1-MALAT1 genomic region appears as a highly integrated RNA processing circuitry critically contributing to immune homeostasis. Its components MEN-β, MEN-ε, menRNA, MALAT1, TALAM1, and mascRNA are obviously set for well-balanced interactions with each other. Genetic ablation of any element therefore leads to major dysfunction.

Supplementary Files

This is a list of supplementary files associated with this preprint. Click to download.

- SUPPLEMENTARYINFORMATION.docx